Mogk, N. 2023. Tapping the hourglass: Disequilibrium relaxation following accelerated nuclear decay. In J.H. Whitmore (editor), *Proceedings of the Ninth International Conference on Creationism*, pp. 327-345. Cedarville, Ohio: Cedarville University International Conference on Creationism.

TAPPING THE HOURGLASS: DISEQUILIBRIUM RELAXATION FOLLOWING ACCELERATED NUCLEAR DECAY

Nathan Mogk, Independent researcher, Tucson, AZ nm8911@gmail.com

ABSTRACT

In 2005, the Radioisotopes and the Age of the Earth (RATE) research initiative published compelling evidence for at least one episode of past radioactive decay which was accelerated by orders of magnitude compared with the rates measured in recent years. Constancy of radioactive decay rates is a central assumption in radiometric dating. Accelerated nuclear decay (AND) causes systematic change in the results of radiometric dating beyond the above normal *in situ* accumulation of daughter products. This includes relaxation of magma reservoirs to equilibrium and excessive inheritance arising from disequilibrium excesses of daughter products of greater order than crystal-melt partition ratios. Uncertainties associated with these mechanisms are shown to disproportionately affect "old" magma reservoirs and magmatic systems that persist after the end of the accelerated nuclear decay epoch.

This paper continues the RATE research by developing a mathematical formalism and deriving several significant equations covering nuclear decay acceleration factors, primordial signature, inheritance, mixing, relaxation to equilibrium, sampling, and measurement which are different from the equivalent relations under the standard assumptions of constant decay rates. This paper identifies steps needed to produce a model of acceleration factors over time that enables the recovery of absolute dates from isotopic analysis under certain circumstances when properly constrained by ongoing and future radiometric and geologic observations. Also discussed are the appropriate conditions and usage for corrected absolute radiometric dating and relatively accurate dating. Statistical variation of isotopes in rocks, discordance, and secular equilibrium data are required for constraining accelerated nuclear decay histories within and across radioisotope systems. The San Francisco Volcanic field is identified as a location with appropriate geological context and some existing radiometric dates to test for the existence of the reservoir relaxation mechanism.

KEYWORDS

accelerated nuclear decay, radiometric dating, excess argon, reservoir relaxation, relative dating, inheritance, corrected dating, partition ratios

I. INTRODUCTION

A. Partitioning and extraneous decay products

Radiometric dating techniques depend on the assumptions of closed system behavior of the rock or mineral to be dated as well as low incorporation of non-radiogenic daughter isotopes to produce reliable dates. (In the case of K-Ar and Ar-Ar dating, zero age is equivalent to an atmospheric Ar isotopic composition (McDougall and Harrison, 1999).) Isochron, laser spot, and step-heating methods are able to partially deal with issues arising from violations of these assumptions, but model ages, which remain by far the most common methodology, depend on the assumption of low extraneous daughter products (Kelley, 2002b). The discussion in this paper is applicable to any radioisotope dating method, but emphasis will be put on the K-Ar system with minor emphasis on the U-Pb system in zircon due to the availability of relevant data and long histories of detailed study. Extraneous daughter products include isotopes inherited from the mantle source reservoir as well as excess incorporated through processes other than *in situ* radioactive decay. The ratio of the concentration of an element in a melt or hydrothermal fluid versus in a mineral is known as the partition coefficient. Radioistope systems used for dating were chosen to have small partition coefficients in commonly dated minerals to ensure that the assumptions required by the techniques were met. In the case of Ar in olivine and clinopyroxene, Ar can be incorporated in the crystal at a ratio of 10^{-3} (Heber et al., 2007), and at ratios of $< 10^{-2}$ in a variety of other minerals (Jackson et al. 2021). In zircon, the partition coefficient of Pb directly grown from melt can be as small as 10^{-6}, up to as high as 10^{-3} depending on the availability of charge balancing ions. When grown from aqueous solutions onto crystal seeds, the coefficient can be as high as 0.25 (Watson et al., 1997). Incorporation of extraneous Ar during crystallization has been demonstrated, and can produce age results that are indistinguishable from a valid age (Scibiorski et al., 2021). Ar in its various mineral contexts and Pb in zircon have some of the smallest partition coefficients for daughter isotopes used in radiometric dating. The partition coefficients directly drive the mechanisms described in this paper, so isotopes with larger partition coefficients are more strongly affected. All are too large to overcome

the excess daughter products produced during accelerated nuclear decay (AND).

Extraneous daughter products, particularly Ar, are a known and well researched topic (see for example Overman, 2013). Technology and knowledge of the behavior of extraneous products has improved since the issue was first encountered, and dates that might once have been discarded are now analyzed to elucidate the crystallization and thermal history of a sample (Kelley, 2002a). Not only isotopes, but entire minerals with their total inventory of radiogenic products can be inherited by a magma (Bea et al., 2021) or metamorphic rock (Sherlock and Kelley, 2002; Giorgis et al., 2000). Much of the excess in the case of argon is known to be concentrated in certain minerals (Harrison et al., 1994; Damon et al., 1967), along grain rims (Lee et al., 1990), and in fluid inclusions (Rama et al., 1965). Techniques, such as *in vacuo* crushing (Hu et al., 2018) and step heating (Holm-Alwmark et al., 2021), have been developed to distinguish supposedly excess Ar from *in situ* radiogenic Ar. Given the preferred partitioning of Ar into fluid inclusions and mineral rims, *in vacuo* crushing allows for the release of the excess without further contaminating the sample with atmospheric argon. The step heating technique for measuring Ar heats the sample slowly in discrete steps which allows Ar in domains near the surface to evolve before that in domains from deeper within the mineral grains. The plateau age is the final age determined from the sample as the most central domains release their Ar. A date may also be obtained from the total amount of gas evolved (Merrihue and Turner, 1966). Laser spot analysis is used on sectioned and polished grains (particularly zircon) to ablate minute amounts of the mineral which is then analyzed for a date. This allows for spatially restricted dating on a fine scale, and mineral rims and cores can be dated separately.

Isochron analyses, which can be applied to any radiometric technique, can also be used to determine the initial amount of daughter products incorporated into the mineral. This is accomplished by trading the assumption of zero initial excess for one specifying that deviations between the radiogenic and non-radiogenic daughter isotope is correlated with the parent isotope through the mechanism of nuclear decay. This alternate assumption is susceptible to mixing effects and may also be negatively impacted by loss or addition of parent or daughter. Extreme excess incorporated on fine scales (smaller than the analysis volume) as a result of AND would not be distinguishable from a valid date for all of the methods described above and for any radioisotope system, though it may still contribute to additional, non-cryptic excess.

B. HISTORIC LAVA FLOW DATA

Snelling (1998) published a list of recent lava flows with known dates from recorded history in which the radiometric ages were greatly inflated. Snelling's list was not exhaustive and did not include all the measurements reported in the references that he included. Instead, he selected measurements which very clearly demonstrated extraneous argon as an issue in K-Ar and related dating methods. Many of the measurements were done early in the development of K-Ar dating, when the techniques to deal with the known issue of extraneous argon were being developed. Some of these measurements also included the glassy rims of pillow basalts (see for example Fisher, 1972). This rapidly cooled glass more closely represents the composition of the melt as opposed to the crystal fraction of solidifying lava, and so would be expected to have a higher excess. Table 1 is an updated list of selected measurements of historic lava flows. There is significant overlap with Snelling's references, but the list has been updated to only provide groundmass measurements with some newer additions. This list of historic flows with anomalously high Ar, similarly, is not meant to be exhaustive or normative. Most historic lava flows correctly yield zero radiometric age, but negative measured ages are also possible (Dalrymple, 1969; Krummenacher, 1970). With modern techniques, dating lava flows in the historical realm is feasible

Table 1. Selected published anomalously old K-Ar dates for historic flows.

Volcano	Flow date	Age (ka)	Reference
Mt St Helens	1986	350 ±50	Austin (1996)
Mt Erebus	1984	48 ±8	Esser et al. (1997)
Mt Erebus	1984	179 ±16	Esser et al. (1997)
Mt Erebus	1984	50 ±30	Esser et al. (1997)
Mt Erebus	1984	640 ±30	Esser et al. (1997)
Mt Erebus	1984	101 ±16	Esser et al. (1997)
Mt Ngauruhoe	Feb 19 1975	1000 ±200	Snelling (1998)
Kilauea	1972	80 ±240	Ozawa et al. (2006)
Mt Etna	May 1964	700 ±10	Krummenacher (1970)
Mt Stromboli	Sep 23, 1963	2400 ±2000	Krummenacher (1970)
Kilauea Iki	1959	8500 ±6800	Krummenacher (1970)
Mt Ngauruhoe	Jul 14, 1954	1000 ±200	Snelling (1998)
Mt Ngauruhoe	Jun 30, 1954	3500 ±200	Snelling (1998)
Mt Ngauruhoe	Jun 30, 1954	1200 ±200	Snelling (1998)
Mt Ngauruhoe	Jun 4, 1954	1500 ±100	Snelling (1998)
Mt Ngauruhoe	Feb 11, 1949	1000 ±200	Snelling (1998)
Mt Lassen	1915	110 ±30	Dalrymple (1969)
Novarupta	1912	2360 ±50	Shormann (2013)
Hualalai	1801	80 ±70	Ozawa et al. (2006)
Hualalai	1801	390 ±30	Ozawa et al. (2006)
Hualalai	1800–1801	300 ±40	Ozawa et al. (2006)
Hualalai	1800–1801	540 ±50	Ozawa et al. (2006)
Hualalai	1800–1801	1410 ±80	Dalrymple (1969)
Hualalai	1800–1801	1600 ±160	Dalrymple (1969)
Hualalai	1800–1801	22800 ±16500	Krummenacher (1970)
Kilauea	> 1800	12000 ±2000	Noble and Naughton (1968)
Kilauea	> 1800	21000 ±8000	Noble and Naughton (1968)
Mt Etna	1792	350 ±140	Dalrymple (1969)
Medicine Lake	> 1500	12600 ±4500	Krummenacher (1970)
Rangitoto	> 1300	150 - 470	McDougall et al. (1969)
Sunset Crater	1064–1065	250 ±150	Dalrymple (1969)
Sunset Crater	1064–1065	270 ±90	Dalrymple (1969)
Kilauea	> 1000	42900 ±4200	Dalrymple and Moore (1968)
Kilauea	> 1000	30300 ±3300	Dalrymple and Moore (1968)
Mt Etna	122 BC	250 ±80	Dalrymple (1969)

(Renne et al., 1997). These observations provide several features that should be accounted for in a radiometric dating framework:

1. Extraneous daughter isotopes are common components of the magma sources of modern lava flows.

2. Most modern flows date correctly to near zero age.

3. Some modern volcanic systems consistently measure with anomalously old ages.

4. Behavior of extraneous daughter isotopes is dependent on the volcanic system.

C. Magma reservoir radiogenic daughter loss pathways

Magma bodies are chemically connected to their immediate surroundings and ultimately the surface via magma/lava convection, diffusion, and dissolution of volcanic fluids and gases (Watkins et al., 2017; Rust et al., 2004). Because radioisotope decay products like Pb and Ar with partition coefficients <1 are preferentially partitioned into fluids and melts, these escaping fluids have the effect of depleting the inventory of daughter products of the magma body over time. If the magma body could be sampled directly, an initial excess would be observed as a steady decrease in the apparent age of the magma over time. Eventually, this would achieve an equilibrium where the rate of removal of decay products is balanced by the production of daughter products via nuclear decay. Decay products are generally trace components of the overall volatile composition and include He and Ar (Cheng et al., 2021). Even lead, as the final decay product of the U and Th decay chains, partitions into volcanic gases, and so will be released to the environment from the magma reservoir over time (Zelenski et al., 2021). Extreme radiogenic excesses of ^{40}Ar that are above the ability of the local radioisotope inventory to produce have been observed (Torgersen et al., 1989), and the production and release of radiogenic Ar has affected the modern atmospheric element ratio with respect to the ancient atmosphere (Renne et al., 2009). Measurements of fumarole gasses are easy to make and abundantly collected at modern volcanoes, however other processes in the magma system are also relevant for reducing large excess of radiogenic daughter products including partial melting and crystal fractionation.

Noble gasses are believed to be reliable tracers of source reservoirs because it is thought that the original inventory of the earth contained very little, and the concentration of each is linked to radioactive decay, either as a direct product of common or extinct radionuclides or by interaction with decay induced thermal neutrons (Graham, 2002; Ballentine and Burnard, 2002; Ballentine et al., 2002). Noble gas studies are often undertaken at active volcanic fumaroles to fingerprint the magmatic source and to identify changes which might lead to an eruption. These studies have shown pervasive mixing of sources and their reconfiguration during the course of seismic or magmatic events (Bini et al., 2022).

The apparent age of a magma reservoir when at equilibrium depends on the efficiency of decay product removal compared to the production rate. It would be expected to vary by volcano and over time but remain generally low for a long-lived magma body under today's slow decay rates. However, during the AND epoch, the ability of magma bodies to achieve equilibrium would be severely restricted, and apparent ages would be significantly above the equilibrium values. Over time, these would relax back to the expected equilibrium values.

Volatile content of the magma, along with depth, overall volume, and cooling rate all determine the overall fluid flux. Intrusion geometry determines the location of fluid release (Lamy-Chappuis et al., 2020; Kawaguchi et al., 2021). In each case, the controlling parameter is specific to the chemistry and geometry of the specific magma body. The pathways that magma and fluids travel to reach the surface can also have a "filtering" impact on the volatile content of the erupted lava (Ubide et al., 2021). Isotopes in fluids will also be fractionated as they travel through and interact with varying geological contexts (Hoang et al., 2021).

D. Prior decay history models

In 2005, the Radioisotopes and the Age of the Earth (RATE) research initiative published multiple lines of evidence that decay rates of radioactive isotopes used in radiometric dating were accelerated with respect to current rates in the past (Vardiman et al., 2005). The same lines of evidence were subsequently used to successfully predict field observations of radiohalos in metamorphic terranes (Snelling, 2008). The RATE authors did not provide tight numerical constraints but indicated that rates were likely accelerated by at least a factor of 10^8 At these great accumulation rates, the amount of daughter products would quickly overwhelm the ability of the magmatic plumbing to keep concentrations at equilibrium values, and they would be inherited by solidifying minerals at anomalously increased rates, commensurate with the relative magnitudes of the decay acceleration and the partition coefficients.

Previous modeling of possible decay histories was first done in the RATE report (Vardiman et al., 2005). The authors proposed a two-pulse model of AND with a single pulse during the Flood accounting for approximately 500 Ma worth of decay, with a gradual ramp-down to modern decay rates in the centuries after the Flood. This was coupled with another, even greater, pulse during the first portion of Creation week, accounting for the remaining 4 Ga worth of decay products, with the Antediluvian period having more or less the same decay rates as modern ones. This model in its essentials is still commonly used by the authors today, as well as others, though some of the original authors have since proposed alternate models. The minor AND ramp-down was proposed to account for the remaining elevated radiometric dates obtained during the post-Flood period. No mechanisms related to the recovery of magmatic systems from the AND epoch were considered (Baumgardner, 2012).

In the same volume, Chaffin (2005) took a theoretical approach to mechanisms which might produce the hypothesized accelerations. Some of the possible mechanisms that he identified generally were characterized by discontinuous jumps of many orders of magnitude as the parameters crossed critical thresholds.

Humphreys (2014) produced an alternate model based on the remnant magnetizations of lunar rock samples obtained during the Apollo program and his model for the free decay of the lunar magnetic field. His updated model retains the single pulse during the Flood of the same magnitude and gradual ramp-down, but replaces the first pulse by a significantly lower level of AND which persists from the Fall throughout the Antediluvian period.

As a follow-on to the RATE study, Snelling (2014) did a thorough review of meteorite dating. Though the results of previous reports on meteorite dating consistently yielded ages of 4.5 Ga, Snelling reported that some of the evidences which were associated with AND in the RATE report, particularly the systematic discordance data were not found. So, Snelling proposed that the meteorites, and the earth by extension, had an initial primordial fine mixture of parent and daughter isotopes that produced a characteristic radiometric age signature. In this case, the Flood pulse and gradual ramp-down again is retained, but there is no AND during Creation or the Antediluvian period.

Since the RATE study, other authors have continued to develop models of radiometric change which do not rely on AND as a primary mechanism. Hung (2008) proposed a sophisticated solute transport model for radiometric change in the U-Pb system undergoing open system behavior. Hung's proposed model is not an applicable explanation for all old radiometric dates, particularly since techniques have been developed to probe the applicability of the assumptions of secular equilibrium and closed system behavior—though these are seldom used in practice. Nevertheless, transport phenomena and Hung's model are likely to have increased applicability following an episode of AND when daughter products are exceedingly abundant. This line of research merits further development. Diffusion along grain boundaries and within the crystal lattice redistributes excess daughter products, especially Ar (Pickles et al., 1997; Reddy et al., 1996). Diffusion controls the closure temperature and in complex systems can be a lower temperature than previously assumed (Nteme et al., 2022).

The RATE study raised numerous new research questions that were not originally addressed in the report or follow-on research by the authors (Froede and Akridge, 2012; Oard, 2013). This paper seeks mathematically to model one such open question on the evolution of magmatic systems that have been subjected to an episode of AND and the consequences for radiometric analyses. Reed and Froede (2010) made a call for an absolute correction factor between radiometric dates and biblical history. They posed several poignant questions regarding how such conversions might be constructed from observations, how they might be validated, and how discrepancies among different radioisotope methods might be handled. I hope that this paper adequately addresses such concerns.

II. DERIVATIONS

A. The decay equation with variable decay constant

I begin by deriving the decay equation without assuming a time-invariant decay rate, as well as developing a formalism for describing episodes of AND. The result is fairly intuitive and matches the usage of the RATE authors, though that study did not provide a derivation. The following derivation also provides a basis for subsequent derivations made in this paper.

First let us assume that the number of parent radioactive atoms, P, in a given rock sample decreases over time at a rate proportional to P. Let us also assume that each decay simultaneously adds a daughter atom to the total number of daughter atoms, D, in the sample. The potentially time variable fraction of radioactive atoms decaying per unit time is defined as $\lambda(t)$. Conventionally, λ is assumed to be constant, and we will derive that as a special case. In all cases t without decoration represents an independent variable. Variables which indicate a particular value of t will include a lower-case or numerical subscript.

$$\frac{\mathrm{d}P}{\mathrm{d}t} = -\lambda(t)P \tag{1}$$

Under standard assumptions, $\lambda(t) = \lambda_0$ is a constant, and the solution to the equation can be written as

$$t_m = \frac{1}{\lambda_0}\ln\left(1+\frac{D}{P}\right), \tag{2}$$

which is known as the dating equation. To account for time variable decay we define an acceleration factor, $\Xi(t)$, as

$$\boxed{\Xi(t) = \frac{\lambda(t)}{\lambda_0},} \tag{3}$$

where λ_0 is a reference decay rate. Because the component decay rates are positive, $\Xi(t)$ must be strictly positive. Additionally assume that $\Xi(t)$ is constructed such that it is piece-wise defined, and integrable over the entire interval.

Conventionally, the quantity t_m above, which assumes a constant decay probability, is understood to represent the radiometric age of a rock sample. However, since λ is a function of t and not constant, t_m is similarly a function of t. Let us introduce a function, $H(t)$, with units of time, that encodes the nuclear decay history. This function which we shall refer to as the Decay History function (also known as the radiometric transfer function) is given as

$$\boxed{H(t) = \int_0^t \Xi(\tau)\mathrm{d}\tau.} \tag{4}$$

The variable t represents an age before present, and so is 0 at the present time and increases looking backward in time. Since Ξ is dimensionless, $H(t)$ has units of time. It represents what we shall refer to as *radiometric age*. The derivation of equations 2, 3 and 4 can be found in appendix section A.

By virtue of definition, $H(t)$ is continuous and strictly increasing with the fixed point $H(0) \equiv 0$. Helpfully, $H(a) < H(b) \Leftrightarrow a < b$, and the function covers every value of both the real time and the radiometric time, therefore $H(t)$ is a bijection, which is a necessary condition for valid relative ordering of radiometric dates. Furthermore, this implies that an inverse to the history function exists, in principle, which can produce absolute dates from radiometric measurements:

Theorem 1. *Given a radiometric history function* $H(t) = \int_0^t \Xi(\tau)\mathrm{d}\tau$ *defined over all* t *such that* $\Xi(\tau)$ *is strictly positive and piece-wise integrable over* $\tau > 0$*, then there exists an inverse,* H^{-1} *such that* $H^{-1}(H(t)) = t$.

As long as $H(t)$ is defined continuously for every possible value of t, then it will be unique for a given $\Xi(t)$ regardless of any discontinuous jumps. When attempting to estimate the form of $H(t)$ from discrete measurements, some ambiguity between measurements arises. I address this situation later. Because of the dependence of H on the

ratio between $\lambda(t)$ and λ_0, a particular decay history function might be applicable only to a single radioisotope system. In such a case, then $H(t)$ will be subscripted with the relevant system.

The accumulated radiometric age of an object at any particular time, t_f, compared to an initial reference time, t_i, with $t_f < t_i$ can be written as

$$H(t_i) - H(t_f). \tag{5}$$

The decay history function tracks the accumulated radiometric age of a particular sample under ideal closed system conditions and a time-varying decay rate. Non-radiogenic perturbations, p_n, however, can produce an apparent age, t^*, which is functionally indistinguishable from a r

$$t^*|_t = H^{-1}\left(H(t) + \sum_n p_n(t)\right) \tag{6}$$

Any apparent age as defined above is dependent on both the time of measurement and the magmatic system, which if it contains excess daughter product, will yield an apparent age greater than the actual age. This is locale dependent, so as a point of notation, t^* may be subscripted with a capital letter to indicate the source or reservoir in view. Additional notation relating to this is developed later.

B. Sampling and mixing relations

Objects (rocks, minerals, etc.) that can be radiometrically dated must be samples from a magmatic source (reservoir) which cooled below the closure temperature at the time of sampling t_s. The measured age of the sample is reset from the reservoir age by a factor of $0 \leq \eta \leq 1$ It is assumed that the system remains closed after this point and accumulates decay products according to the decay history function thereafter. The apparent measured age of the sample can be written in terms of the reservoir apparent age, t_P^*, and the time of sampling as follows:

$$\boxed{H\left(t_s^*|_{t_s}\right) = \left[H\left(t_P^*|_{t_s}\right) - H(t_s)\right]\eta + H(t_s).} \tag{7}$$

The same can also be written in the below alternate form:

$$H\left(t_s^*|_{t_s}\right) = \eta H\left(t_P^*|_{t_s}\right) + (1-\eta)H(t_s). \tag{8}$$

This relation provides a general framework for modeling reservoir differentiation from a common source, mixing between multiple reservoir sources, inheritance of radiogenic daughter products into a rock, primordial radiometric signatures, and literal sampling from a rock or lava. In the limits of $\eta \to 0$ or $H(t_P^*|_{t_s}) - H(t_s) \to 0$, then there is no significant inheritance, and $t_s^*|_{t_s} = t_s$. However, for reservoirs with a large radiometric age, significantly older than the time of sampling, then inheritance will be a factor, particularly if $H(t_P^*|_{t_s})\eta$ is greater than the analytical uncertainty of the isotopic measurement. In this case the amount of inheritance is sensitive to the time evolution of the reservoir apparent age. These situations are expected to be common as a result of AND. One strong implication is that inheritance is more likely to be worse for later emplaced samples than earlier emplaced samples during the AND epoch, as $H(t_s)$ decreases quickly. After the epoch, the $H(t_s)$ remains relatively fixed, and the inheritance behavior is dominated by the reservoir evolution.

Reservoirs are themselves sampled from older reservoirs all the way back until one reaches a primordial apparent age, t_Ω^*. Magma reservoirs have an additional evolution applied to their apparent ages as described in the next section. In general, for workable radioisotope systems, the emplacement efficiency will be small, and therefore inheritance from a generation before the immediate source can be safely ignored, although daughter products may accumulate and persist in a melt.

In general, the emplacement efficiency, η, is related to the partition coefficient and is dependent on the pressure, temperature and chemistry during emplacement, so is dependent on the particular magmatic system in view. It is also likely to include a small random component.

Partitioning at a particular time can be modeled by a set of samples, each with a separate inheritance parameter, η_n such that

$$\sum_n \eta_n = 1 \tag{9}$$

The inheritance relation above can be generalized to represent the generation of a sample or reservoir as the mixing of two (or more) different parent reservoirs. After all, inheritance can be thought of as the mixture of a mature source with a juvenile source. The inheritance for some sample, C, derived as a mixture of sources A and B with some mixing parameter $0 \leq \alpha \leq 1$ can be written as

$$H\left(t_C^*|_{t_s}\right) = \alpha H\left(t_A^*|_{t_s}\right) + (1-\alpha)H\left(t_B^*|_{t_s}\right). \tag{10}$$

Mixing may be calculated in a chain to produce any arbitrary mixture of multiple sources. A general form to accomplish this in a single calculation is left as an exercise to the reader. The relations derived above implement potential models 1, 3, and 4 proposed for Ar loss from the Cardenas Basalt by Austin and Snelling (1998).

C. Reservoir relaxation

Consider a homogeneous reservoir of magma which is in communication with its environment and which contains an excess of daughter products arising from a process like crystallization and expulsion of incompatible daughter products or an episode of accelerated nuclear decay. While these daughter products are still in the magma, they are available to be incorporated into samples through inheritance, but over time, the reservoir will release these into the environment. Enhanced inheritance from large excesses of daughter products is a perturbation to the radiometric age of samples taken from the reservoir. Radiogenic products released to the environment decrease this effect, causing an apparent downwards trend of radiometric age of emplaced samples with decreasing closure time that is not directly radiogenic in cause. This excess cryptic inheritance which decreases over time due to the return of the source reservoir to chemical equilibrium is here termed reservoir relaxation. “Relaxation” as a term is used in the fields of chemistry and dynamical systems to refer to a system returning to its equilibrium state after being affected by a perturbation, and I adopt that usage here.

The change of the perturbation caused by excess daughter product can be modeled as proportional to the excess present at any given time compared to the equilibrium value, which is assumed to be 0 — i.e., modern reservoirs should tend towards measuring modern ages. This can be written as the measured unperturbed reservoir age at time t from equation 5, for an apparent initial reservoir age, $H(t_R^*|_{t_s})$ (from equation 7), less the amount of excess that has already been removed by the perturbation $p_r(t)$. The constant of proportionality, β, is the relaxation parameter.

$$\frac{\mathrm{d}p_r}{\mathrm{d}t} = -\beta\left(H\left(t_R^*|_{t_s}\right) - H(t) - p_r(t)\right) \qquad (11)$$

The solution to the above equation yields two contributing relaxation perturbation terms. The first (p_i) is related to the relaxation of the initial excess present in the reservoir and the second (p_x) is the relaxation of additional excess generated during accelerated nuclear decay. The derivation of these perturbations is derived by solving equation 11 in appendix section B. These perturbations represent additional daughter product incorporated into rock samples which decrease in magnitude in later samples as the magmatic reservoir loses its excess daughter product.

$$\begin{aligned} p_i(t) &= H\left(t_R^*|_{t_s}\right)\left(1 - e^{-\beta(t_s - t)}\right) \\ p_x(t) &= -\beta e^{\beta t}\int_t^{t_s} e^{-\beta\tau}\,H(\tau)\mathrm{d}\tau \\ p_0 &= \eta\left[H\left(t_P^*|_{t_s}\right) - H(t_s)\right] = H\left(t_R^*|_{t_s}\right) - H(t_s) \end{aligned} \qquad (12, 13, 14)$$

Subtracting the above two perturbation terms and adding the contribution from inheritance (p_0) from the parent reservoir, P, the total accumulated radiometric age of a reservoir at any given time can be written as

$$\boxed{H(t_R^*|_t) = H(t_s) + p_0 - p_i(t) - p_x(t)} \qquad (15)$$

Because the inheritance and relaxation of a reservoir system are locale dependent, each reservoir will necessarily have a unique function satisfying the above equation. For the sake of notational clarity, let us introduce the Total Radiometric Response function defined as follows:

$$H^+(X,t) = H(t_X^*|_t), \qquad (16)$$

where X is the particular magmatic system under consideration.

Given that $H(t_R^*|_{t_s}) - H(t) \geq 0$ and $-p_r(t) \geq 0$, then $\frac{\mathrm{d}p_r}{\mathrm{d}t} \leq 0$, and $p_r(t)$ is monotonic. Because its contribution to the total radiometric response is either 0 or in the same direction as $H(t)$, and equation 15 covers the entire lifetime of the reservoir and is strictly increasing, $H^+(X,t)$, therefore, is a bijection and can be inverted over the lifetime of the reservoir, for a fixed magmatic system, X.

The above relaxation relation is fundamental to the response of a magmatic system undergoing AND. The only additional assumption admitted was that the relaxation of daughter products in a reservoir back to equilibrium can only happen at a finite rate.

Figure 1 for a hypothetical decay history, illustrates the relationship between the theoretical radiometric age at the true age of closure (t) arising only from AND ($H(t)$), measured radiometric age ($H(t^*)$) and the associated apparent closure time (t^*), and the total radiometric response ($H^+(X,t)$) which accounts for extraneous daughter products present in the sample at the true closure time.

D. Python Implementation

I have developed a Python implementation of the relations defined in this paper at the following link: https://github.com/nmogk/radiometric-tf. The implementation provides a Python package as well as a command line interface that allows a user to load a decay history model file, obtain overall information about its behavior, generate plots of radiometric versus calendar time, and convert between individual radiometric dates and calendar dates, including handling of uncertainties. The command line interface includes help information. Code relating to the decay history function and the command line interface are in the rtf.py file. The rrelax.py file implements the sampling and reservoir relaxation relations and allows modeling of the locale-dependent inputs to total radiometric response, including reservoir relaxation.

The repository also includes five model definition files. Three represent the as-published models of Vardiman, Snelling, and Chaffin (2005), Humphreys (2014), and Snelling (2014). Two others are end-member models of AND which have a single pulse during the Flood which include Precambrian radiometric dates. The accuracy of absolute dates produced with the implemented models depends heavily on how well the models of decay history and reservoir pa-

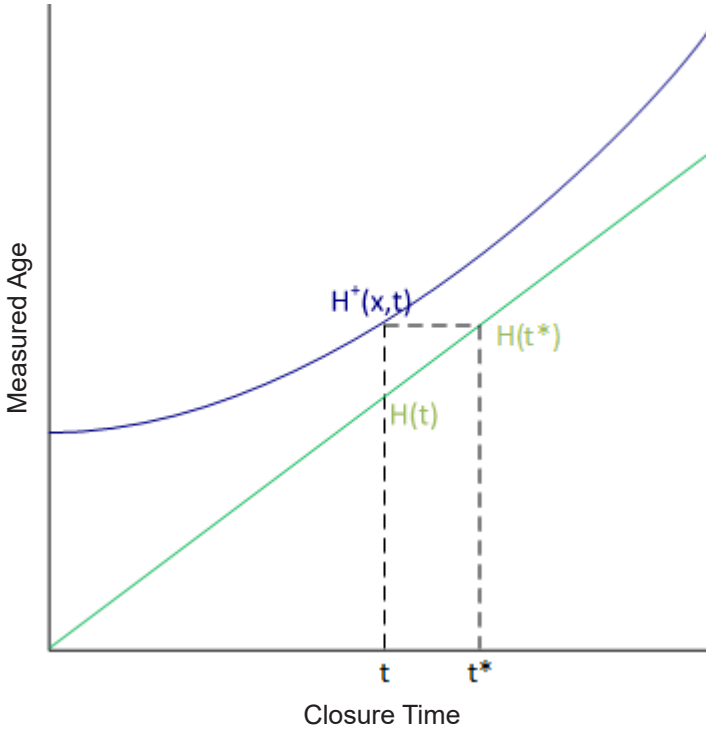

Figure 1. Schematic graph illustrating the relationship between the total radiometric response function, $H^+(X,t)$, the decay history function, $H(t)$, and the maximum closure time, t^*.

rameters (inheritance and relaxation) are constrained in the context of the radiometric measurement.

E. Conditions for relative dating

As previously discussed, in an unperturbed system only subject to the decay history function, which is a bijection, the ability to derive an absolute date from a measurement is guaranteed. Similarly, over the lifetime of a single reservoir (as defined by a single inheritance value and relaxation parameter), the Total Radiometric Response is a bijection which allows for relative dating between samples of the reservoir.

However, when comparing samples from different sources with potentially different reservoir relaxation parameters, then direct comparison can only be made if certain conditions hold. Without loss of generality for two sources, *A* and *B*, relative dating can be guaranteed for any two samples if the following condition holds:

Relative Dating Condition 1.

$$H^{+}(A,t_2) > H^{+}(B,t_1) \Leftrightarrow t_2 > t_1. \qquad (17)$$

In the absence of perturbations, $H^{+}(X,t) \to H(t)$, then the bijective property of $H(t)$ automatically satisfies condition 1. This condition may or may not be met between different isotope systems in general, as it is unknown at this time if all radioisotope systems had the same acceleration factor functions, even if the condition would otherwise be met. The implication is that the most likely situation for this condition to hold is when comparing radiometric dates from the same magmatic system with the same radioisotope system originating during the same time period $A=B$. The above condition is not met in the general case for systems with different magmatic histories, even though both are subject to the same decay history function. It can clearly be seen, however, that this condition does hold if it can be established that $H^{+}(A,t) = H^{+}(B,t)$.

All is not lost, however. A condition for restricted relative dating applicability can be applied to a single source in relation to another over a restricted interval $t_0 \le t_1, t_2, \le t_3$ given by

Relative Dating Condition 2.

$$H^{+}(A,t_2) > H^{+}(B,t_1) \Rightarrow t_2 > t_1. \qquad (18)$$

This condition applies when the total radiometric response function associated with reservoir *A* is always lower than reservoir *B*, i.e., for any two samples erupted at the same time in history, the measured radiometric age of the one associated with reservoir *B* is always the higher one. In this case, relative ordering can be maintained in a one-sided fashion. *B* being older than *A* does not provide relevant chronological information, but if *A* measures older, then it is guaranteed to be older than the same numerical measurement of *B*. The inverse is also true, *B* measuring younger can guarantee that it is in fact younger. This condition possibly provides the easiest method of establishing its validity during field studies.

Finally, even in the case where neither condition will hold for any possible sample time, it is possible that relative ordering of dates will hold if the available samples from each source are sufficiently sparse so as to overcome the maximum size of the ambiguity arising from differential reservoir relaxation parameters. This is the case if, for all samples of *A* and *B* adjacent in time, the following holds:

Relative Dating Condition 3.

$$H^{+}(B,t_2) - H^{+}(A,t_2) < H^{+}(A,t_2) - H^{+}(A,t_1) \qquad (19)$$

Relatively accurate radiometric dating is necessary, but not sufficient for absolute dating. Relative dating holds, particularly if the relative dating condition 1 is applicable, even without knowledge of the form of the decay history function. If the decay history function can be identified, then absolute dating becomes possible. In the case of a system with inheritance or significant reservoir relaxation, then it is necessary to determine the total radiometric response function for the system to achieve absolute dates.

When comparing radiometric dates of samples from two different systems in the general case where inheritance and reservoir relaxation are significant factors, then the total radiometric response function must be known for both systems for both relative and absolute dating. If this is not achievable, then to use relative dating, one of the less stringent conditions listed above must be shown to hold for the systems in question.

III. ILLUSTRATIVE EXAMPLE

The flexibility and behavior of the above derivations are best exposited with a concrete example. The Python implementation of the above equations was used to produce an example model.

The example will assume a radiometric history function of the form:

$$H(t) = \frac{a}{2}\left(1 + \operatorname{erf}\left\{\frac{1}{b}(t-c)\right\}\right) + t \qquad (20)$$

which encodes a single bell-shaped pulse of accelerated nuclear decay where a is the total accumulated age of the pulse, b is a parameter controlling the pulse width, and c is the center of maximum acceleration. The example uses the following parameters:

$a = 4\,\text{Ga},\ b = 0.294\,\text{yr},\ c = 4301.1816\,\text{YBP}$ (Illustrative model 1)

The value of c is 66 ⅓ days prior to the start of the Flood, which for simplicity, is assumed to be 4301YBP.

A history is chosen for the example and described in figure 2 which illustrates several different features of the mathematical formalism derived previously. In it, we begin with a primordial magma reservoir which does not have any inherent age signature. AND begins slightly before the Flood. At the start of the Flood, a parent magma reservoir is differentiated from the primordial reservoir with one tenth of the contemporaneous age signature of the primordial reservoir. Midway through the Flood, this parent reservoir is partitioned into two derived reservoirs, *A* and *B*. The partitioning is accomplished by distributing all the accumulated daughter from the parent into one or the other. This is seen by the unity sum of emplacement efficiency parameters (η). Each reservoir has unique relaxation behaviors with *A* relaxing at a slow rate, and *B* relaxing at an elevated rate. Each reservoir is regularly sampled and measured. The samples do not relax, but they do continue to accumulate daughter products from AND. At the end of the Flood, reservoir *B* begins to relax more slowly, though still more quickly than *A*. The successor *B* reservoir contains the entire age signature accumulated by *B*. Samples are again regularly taken from the reservoirs to show the change in radiometric dates

over time. Note that there is no AND after the end of the Flood, but the radiometric dates of subsequent samples continue to evolve over time due to the reservoir relaxation mechanism.

Figure 3 is a plot of the hypothetical measured radiometric ages for each of the reservoirs in the example measured continuously for all times. The plot domain covers the assumed Flood date and some time before and after. The units are years before present, so history proceeds from right to left. The lines are equivalent to taking a chilled sample of magma for every time and radiometrically dating it *immediately* at the time of sampling, rather than waiting until the present time. So, no additional nuclear decay products would be added before measuring the date. Figure 3 illustrates all the fundamental relations that were derived in this paper. The primordial reservoir is unperturbed during the entire history of the example, so evolves exclusively according to the decay history function. It also represents the maximum age that any derived reservoir can take, since perturbations from the decay history function can only decrease the amount of radiogenic daughter product available. Even inheritance can only provide excess daughter up to that which is available in the parent. All other reservoirs and samples evolve according to the universally applied decay history function while they are not perturbed, and so parallel the primordial reservoir line. This example was not run with a primordial signature so the primordial reservoir line begins at zero radiometric age at the beginning of history. A non-zero primordial

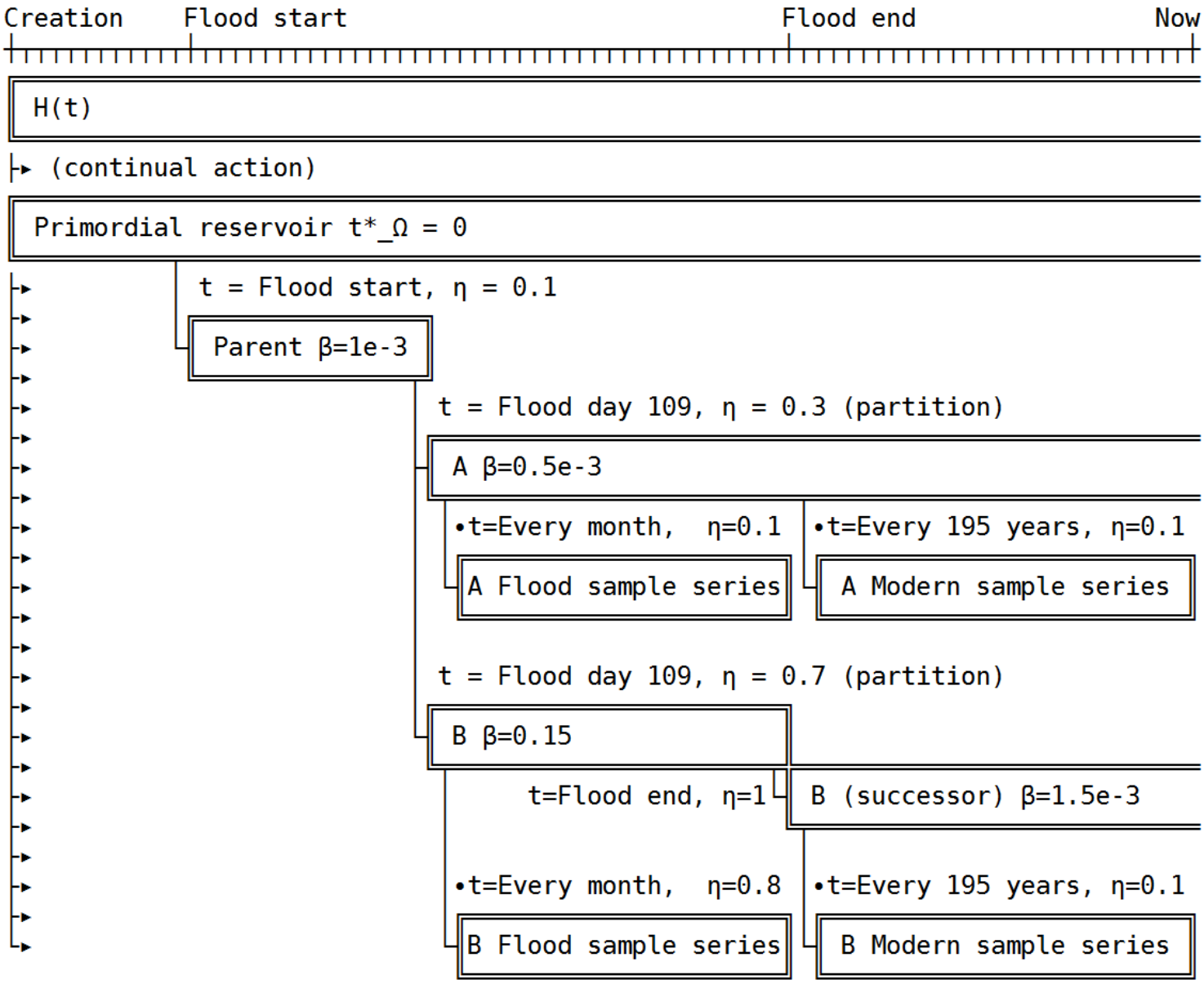

Figure 2. Event stratigraphy of the example network. The single decay history function is applicable for the entire history, and acts continuously on all of the other objects. The network begins with a primordial reservoir with a zero initial age. At the beginning of the Flood, a reservoir is sampled from the primordial one with 10% inheritance. About a third of the way through the Flood, this reservoir is partitioned into two daughters, one of which undergoes a period of rapid relaxation during the Flood. Samples with 10% inheritance (for example, lava emplacement), are taken both during and after the Flood with the exception of reservoir B, which has 80% retention during Flood samples.

signature would manifest as a constant vertical offset on the primordial reservoir line. Sampling from a reservoir can be seen as a vertical drop in the measured age. The derived reservoirs are subject to relaxation, but only in the case of the rapid relaxation of reservoir *B* is it easily visible at this time scale. Samples which do not relax are taken from the derived reservoirs at their differentiation to show the effect of relaxation back to equilibrium on the reservoirs.

Figure 4 shows the same reservoirs as figure 3, but the domain is expanded to include all of history. At this time scale, the effects of relaxation on the reservoirs are more readily apparent. Two samples are taken of reservoir *B* at its original differentiation as well as at the end of the Flood when the smaller relaxation regime takes effect. The difference between the two sample lines shows the total effect of the high relaxation rate during the Flood.

Figure 5 shows the hypothetical measured radiometric ages of the decay history function, reservoirs *A* and *B*, as well as samples taken from the reservoirs. In contrast to figures 3 and 4, the measurements in figure 5 are taken at the present time, having accumulated their full contingent of radiogenic daughter products since the "sampling" time listed on the domain. The domain of the left panel covers the modern era, and the right panel covers the Flood. The samples taken in this example in the modern era have realistically low inheritance from the parent reservoirs, so even though the reservoirs retain a significant fraction of their original decay product inventories, the samples have plausibly low dates. The parameters chosen for the two reservoirs illustrate how the relaxation mechanism can cause relative dating to be inaccurate between different magmatic systems, even when they are subject to the same decay history and inheritance regime. The two series of samples also demonstrate one magmatic system which exhibits elevated radiometric dates from modern eruptions (Res *A* samples), and one which measures correctly at zero. Both systems exhibit dates in the immediate post-Flood period which are greatly inflated, and which decrease with decreasing stratigraphic position, as is observed with real volcanic systems. For the samples taken during the Flood, inheritance for samples taken from res *B* are much greater than those taken from res *A*. This illustrates that having high inheritance causes sample behavior to couple more strongly to the parent reservoir conditions, whereas low inheritance causes samples to be more strongly coupled to the underlying decay history function, as expected.

Figure 6 shows how the samples would be converted to absolute dates if inheritance and reservoir relaxation are not taken into account. Under these assumptions, the corrected sample dates can only be interpreted as maximum closure ages. In all cases, the time of

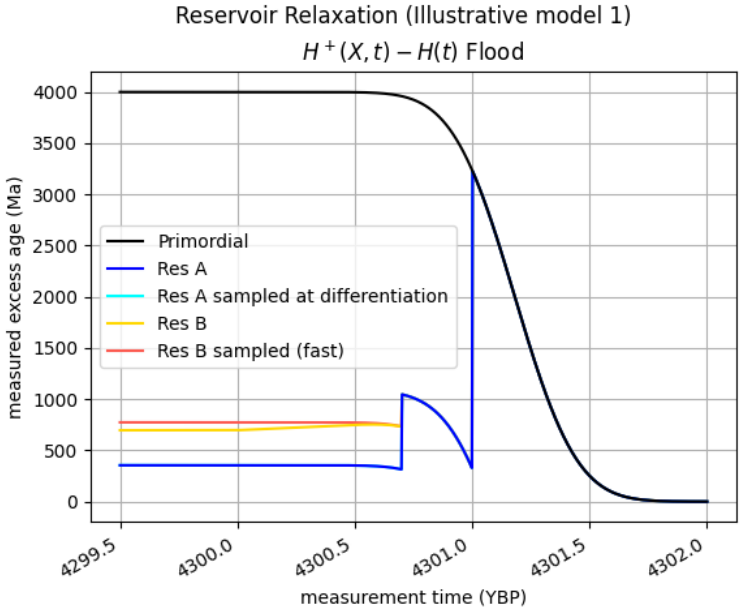

Figure 3. An example system of reservoirs displaying a variety of relationships and behaviors that are possible to model with the equations derived in this paper. The network shown begins as the primordial reservoir with no initial radiometric age. At the beginning of the Flood, it is sampled with 10% inheritance. Later, this reservoir is partitioned into two sister reservoirs, each containing a fraction of the accumulated daughter product at a 30-70 split. Both differentiated reservoirs are undergoing relaxation, but the yellow reservoir has a relaxation parameter 100x greater than the blue one. A sample which does not have any relaxation behavior associated with it of reservoir *A* is taken at the time of differentiation. During the accelerated nuclear decay epoch, the relaxation behavior is too small to observe at this scale (cyan line). The *y*-axis is the total radiometric response less the value of the decay history function. This is equivalent to a chilled sample being taken and radiometrically dated at each point in history.

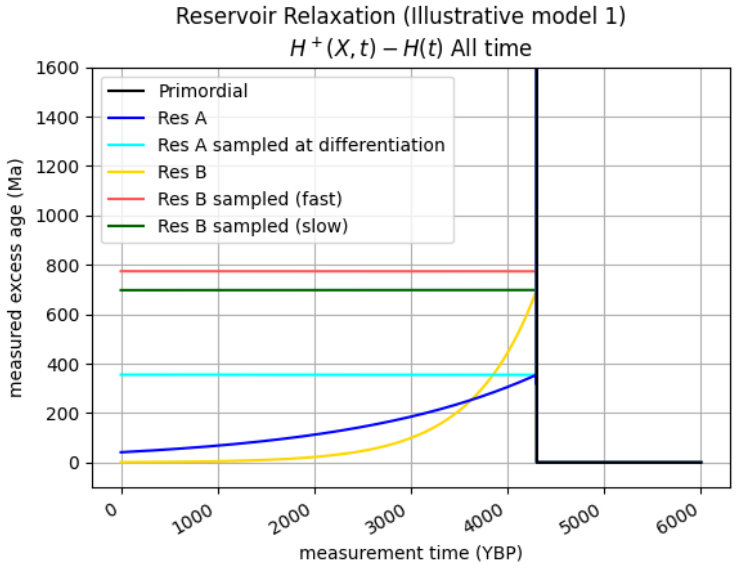

Figure 4. This is the same system described in figure 2 and shown in figure 3, but with the domain expanded to all of history including the modern era. The dates on the vertical axis shown are the dates that would be obtained if measured at each point in history on the horizontal axis. Modern dates are indicated by the intercept of each line with the vertical axis. The rapidity of events during the Flood prevents seeing any detail, but the evolution of the systems over time can clearly be seen. The relaxation behavior of both reservoirs *A* and *B* can clearly be seen with reservoir *B* having a faster relaxation time. Because of this, these two systems violate relative dating conditions 1 and 2, so their radiometric dates cannot be meaningfully compared in a relative sense without knowing the total radiometric response of both systems. Reservoir *B* undergoes two different relaxation regimes during the Flood. Samples (non-relaxing) are taken at the beginning of both the fast regime (red line) and the slower regime (green line) to show the effect that relaxation had during the Flood. The cyan line is a sample taken from reservoir *A* which also reveals the effect of relaxation.

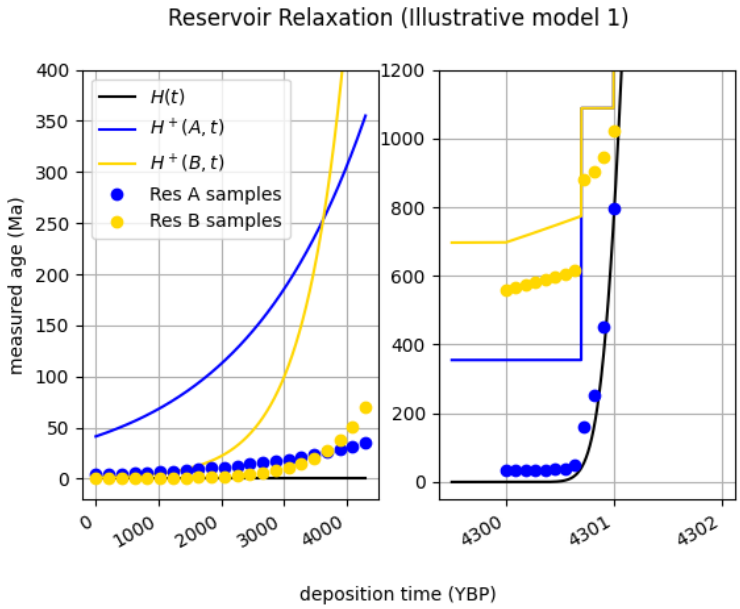

Figure 5. Modern measured age of reservoirs and samples from the system in figure 2 showing long-term evolution. During the Flood, reservoir *B* samples (yellow circles) have significantly higher inheritance, and show increased sensitivity to differentiation and relaxation than reservoir *A* samples (blue circles), which have low inheritance and largely stay close to the unperturbed decay history (black). Because of its faster relaxation, reservoir *B* presently yields zero age radiometric dates for modern flows, but reservoir *A* retains a small excess.

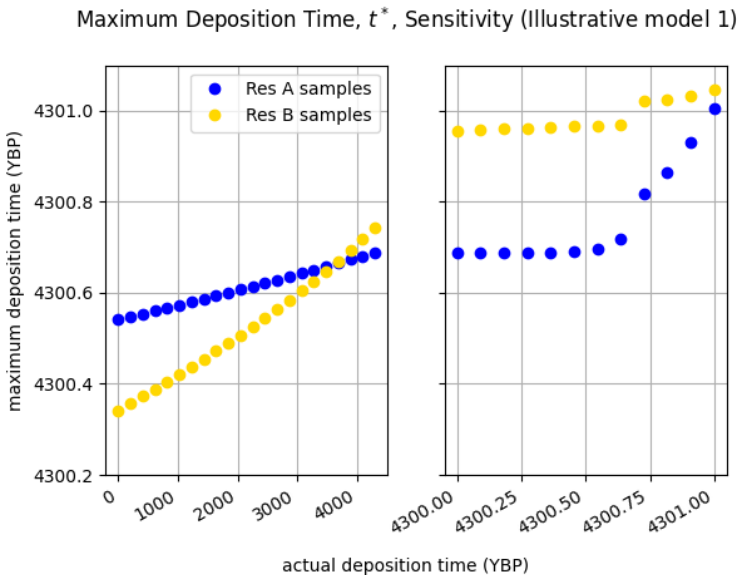

Figure 6. This figure shows the sensitivity of correcting radiometric measurements with unknown perturbations. Each point represents the same samples as in figure 5 with the radiometric date inverted with the known decay history function, and the time interpreted as a maximum deposition age. All of the samples are legitimately interpreted as having formed during the Flood. Only in the case of the pre-differentiation reservoir *A* samples is the maximum date close to the true date. So without knowledge of the relevant perturbations, a single end-Flood radiometric age cannot be determined. The discontinuity in the dates for reservoir *B* come from the change in inheritance, but is not present for reservoir *A*. A smaller discontinuity is seen earlier on related to the partitioning of daughter product between the two reservoirs.

the Flood is included in the possible closure dates. This illustrates the difficulty in distinguishing late- versus post-AND dates without constraining the total radiometric response of a particular volcanic system.

Figure 7 depicts the decay history model proposed in Humphreys (2014) which accounts for the Precambrian accumulated radiometric age with a low level of persistent decay acceleration throughout the Antediluvian period and culminating with a single pulse over the year of the Flood.

IV. DISCUSSION

The reservoir relaxation mechanism proposed in this paper obviates the need for a gradual ramp-down of AND, as this will naturally occur post acceleration epoch, while still reproducing the anomalously old measured ages from the immediate post-Flood era, from volcanoes erupted long after the AND epoch. There may still be evidence of post-Flood AND in the ratios of cosmogenic radionuclides which are commonly used for Quaternary dating (Oard, 2021).

This mechanism also explains why some modern magmatic systems produce anomalously high dates while others produce sensibly modern dates.

The mechanisms described above which are able to remove daughter from a sample are limited to achieving zero age at minimum. Therefore, any radiometric date measurement must yield a date that is at most as young as the actual closure date (ignoring any possible open-system behavior, and allowing for analytic uncertainties). Therefore, t^* is a maximum closure age. This can be a useful metric for determining the relative ordering of geologic events, given the further discussion below.

Given the definition of the Radiometric History Function, including the assumption that the acceleration is uniform in space, then there

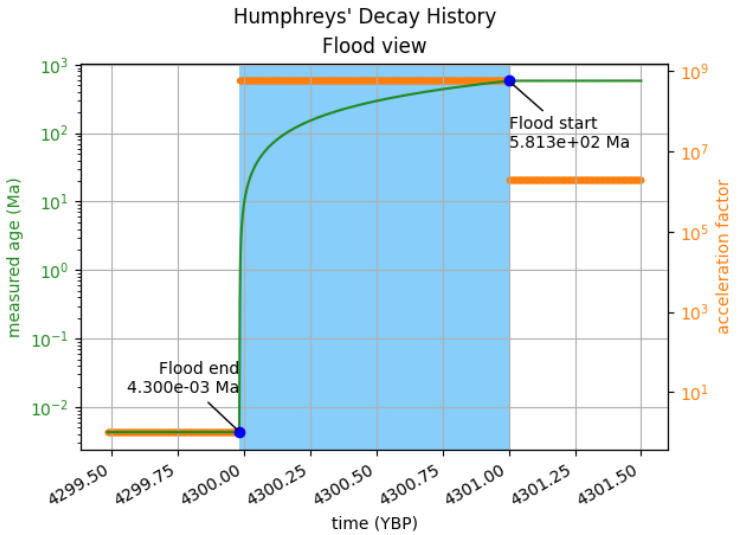

Figure 7. Acceleration factors and radiometrically measured ages for materials with closure ages at all times around the time of the Flood according to the model proposed by Humphreys (2014). This model consists of acceleration factors in three regimes, the modern one, a significant pulse during the Flood year, and a long-lived lower acceleration regime during the Antediluvian period.

is a one-to-one correspondence between historical dates and radiometric dates. If different isotope systems have experienced different acceleration histories, then the same would apply to each system, though they may be different from each other. Two important aspects of the relations derived in this paper are locale dependent. The first is the sampling relation, which depends on time, temperature, chemistry, and source history of the magma (Karpinskiy et al., 1966). Successive sampling events geometrically reduce the influence of earlier ones, so for the low inheritance expected for workable radioisotope dating systems, prior sampling can likely be safely ignored. Conditions where anomalously high incorporation of extraneous daughter products occur are, however, more likely during and following an AND episode. Significantly different sampling (inheritance) behavior between two different localities can prevent dates from being strictly equivalent to each other and thereby violate the conditions for relative dating.

The other locale-dependent factor is the relaxation parameter, β, which is certainly dependent on location and may also be dependent on time as a magma system is reconfigured and takes on new connection characteristics with respect to the environment (Byrne et al., 2021; Geist et al., 2021; Day and Hilton, 2020).

For

$$\Xi(t) \gg \beta T, \tag{21}$$

(where T is a timescale of interest) reservoir relaxation is an insignificant contributor to the variability of measured radiometric ages over closure time. This changes, however, post-acceleration epoch as decay acceleration decreases to 1 and timescales increase. This introduces a pitfall for measuring corrected ages near or after the end of the Flood. The exact behavior of the system will depend on the relative rate of change between $H(t)$ and the size of β. During the accelerated nuclear decay epoch, reservoir relaxation is likely to be very small compared to the accumulation of decay products and is likely insignificant. After the epoch, however, when a large excess of radiogenic daughter products is present, and with sufficient time for relaxation back to equilibrium to occur, the secular change in cryptic inheritance of measured ages will increase. Because the rate of change in inheritance caused by reservoir relaxation depends on the geological configuration, it cannot be guaranteed that radiometric dates from different magmatic systems are equivalent. As a consequence, late Flood and post-Flood may not be practically radiometrically distinguishable. Within the same system, the relaxation perturbation causes a decrease in the measured ages in the same direction as the decay history function over time, so their sum remains a bijection, and relative dating will still work, but only for samples sourced from systems which share reservoir ages and relaxation parameters. To determine absolute ages or to reliably determine relative ages across two different systems would require knowledge of the relaxation history of each system involved.

Rocks which formed pre-epoch would not be subject to the secondary processes of reservoir relaxation and inheritance which redistribute radioisotope products, and so should date very consistently with each other. Another case with practicable application is plutons and associated volcanic rocks which underwent rapid cooling, fast enough to prevent relaxation back to equilibrium from changing the isotopic inventory of the reservoir. In this case, inheritance is likely to be a dominant effect, but if the degree of inheritance can be determined, or localized and excluded, then such plutons would provide useful fixed points.

A. Developing and calibrating radiometric histories

The promise of corrected absolute dating depends on the establishment of reliable decay history functions, with time indexed constraints on $\Xi(t)$ for specific radioisotope systems. Several lines of evidence are important to defining and constraining these models through time. These include radiometric tie points that can be determined from other lines of evidence, time series radiometric gradients, determination of natural variability of isotopes in rocks, measurements of departure from secular equilibrium, discordances between radioisotope systems and alternate chronometric systems. Literature reviews or measurement campaigns should be carried out to identify the implied constraints on the mechanism and history of decay acceleration.

Because the processes described in this paper produce variable and sometimes contrary effects on the measured ages of datable materials subjected to AND, full calibration of a comprehensive decay history model is a difficult and synthesis-level effort. It is far from intractable, however, by taking an iterative approach to constraining the globally applicable decay history function versus the locality-specific parameters. Datable geologic materials are subject to the total radiogenic accumulation of daughter products from the time of their crystallization going forward, so working backwards in time is necessary to completely account for a radiometric age. However, following from the definition in equation 1 the acceleration function may be determined independently for any subset of time without reference to later events. This is useful, since volcanoes in the post-Flood period are most susceptible to the complications arising from the relaxation mechanism. The RATE authors developed four potential methods for constraining the acceleration function by the Po production requirements for the presence of Po radiohalos (Snelling, 2005), ^{14}C in geological materials (Baumgardner, 2005), induced fission, and Po radiohalo energies (Chaffin, 2005).

With continuous measurements of $H(t)$, the acceleration factor function can be uniquely determined, but some ambiguity arises in the case of having only discrete measurements available. An example of this is shown in figure 8. For a single radiometric measurement from a particular time, t_a, there are multiple acceleration histories which could plausibly result in the same $H(t_a)$, and we do not know *a priori* which one we should choose. In general, at a different value of $t = t_b$, different acceleration histories will produce different values of $H(t_b)$. Therefore, to constrain the particular acceleration function, radiometric measurements from multiple different crystallization times must be analyzed. There will still remain some ambiguity where there are gaps in sampled times, but the uncertainty decreases as spacing between measurements decreases. Between sample times, the interpolated acceleration function represents the average value over the interval, which in most cases is likely to be a reasonable approximation.

The most fundamental step in constructing a reliable decay history is to establish fixed points in the stratigraphic record which reliably

correspond to Biblical events, particularly the beginning and end of the Flood and Creation. The acceleration function can be determined directly through time series measurements of deposits which were repeatedly laid in succession from the same volcanic system during the Flood. Examples include mid-ocean ridge basalts, large igneous provinces, or multiple sill/dike intrusions for which the stratigraphic ordering can be independently determined. For such deposits, each individual deposit should be subject to approximately the same inheritance, and changes due to reservoir relaxation during the Flood should be generally low. The decay acceleration can then be determined by the difference in measured ages over the time interval to within two orders of magnitude, which can then be tightened by coupling with a kinematic model of deposition timelines. Once multiple values of $\Xi(t)$ can be determined, new measurements can be fitted to times with the same regime, and inheritance and relaxation parameters can be determined.

With a large number of determinations made at various localities of the Flood initial and terminal boundaries, radiometric boundaries can be determined. Analysis of multiple rocks laid down during the last portion of the Flood would then yield the overall total amount of post-Flood acceleration, since all would be subject to the same modern era decay product accumulation. This set would also yield typical inheritance regimes for Flood rocks. A similar statistical treatment of modern volcanoes, assumed to have substantially similar relaxation parameters per volcano type (i.e., subduction stratocone, basalt monogenetic, hotspot, etc.) would yield typical cryptic inheritance parameters, which can then be used to analyze specific systems for locale-dependent relaxation parameters and provide constraints on the post-Flood decay acceleration regime. Maximal inheritance could also be established, and with the measurements from the youngest Flood rocks, a radiometric post-Flood/Flood boundary could be determined along with any overlapping ambiguous range, if one exists. More detailed modeling of variable decay during the Flood can be made by adding additional fixed points to more chronological events,

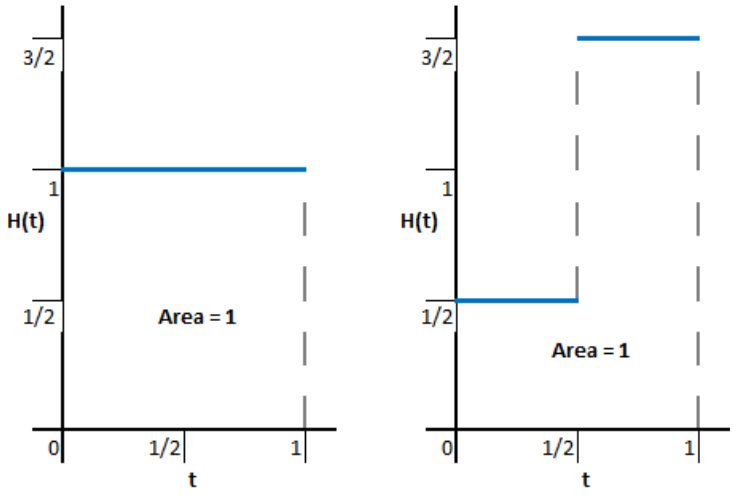

Figure 8. $H(t)$ is an integral over the decay accelerations experienced since crystallization. This can be represented geometrically as the area under a curve. The two curves above have the same area and represent two possible acceleration histories that yield the same radiometric age at point $t = 1$. The areas are different for any other value of t.

or by using kinematic models of the Flood to interpolate between events. Continued theoretical work on the mechanism of AND might constrain the total number of rate determinations that must be made.

Relaxation and excess inheritance parameters for individual magmatic systems will be difficult to determine initially before a well-supported decay history model is in place to subtract out the effects of AND. This potentially presents a bootstrapping problem, since all real measurements will be subject to their magmatic system's unknown equilibrium condition, which in general are unavailable to direct measurement in either time, space, or both. An initial recommendation for the ordering of the overall synthesis was given above. In the case of individual rocks in particular systems, there are a variety of potential observations which will help to separate and estimate the inheritance and relaxation parameters. In the case of historical eruptions of single volcanoes with sufficient eruptions and historical timing constraints, the value of the relaxation parameter can be directly fit. Using the data from Kilauea in table 1, yields a K-Ar relaxation parameter value between $0.2 \cdot 10^{-2} - 1.5 \cdot 10^{-2}$/year, though this is likely to be unreliable due to the quality of some of the measurements. More recent, high-quality measurements from multiple radioisotope systems will be needed. Fumarole and spring data, along with tomographic measurements of magma chambers and seismic data can be used to estimate the relaxation parameters of currently active volcanic systems.

For extinct volcanic systems, some elements of the total system are no longer available for observation, but there is in many cases good exposure of plutonic systems. Some exquisite geological sites offer the opportunity to study rocks from different levels in the magmatic system, and can provide information about the final partitioning between different minerals and magma constituents. Plutonic data is particularly important for the U-Pb system in zircon and other systems where the closure of the crystal system happens in the magma chamber. Many mining districts have detailed observations of plutonic complexes and their associated hydrothermal systems. An estimate of the total inventory of daughter products provides an estimate of the initial inheritance parameters and can be used as a starting point to determine the relaxation parameter.

Radiometric dating is usually carried out a small number of times for a single rock, often once, with additional analysis resources mostly being devoted to dating other rocks to determine the age relationships among them. Recently, reduction in cost of doing multiple analyses has led to a more statistical use of zircons in detrital sediment studies. Uncertainty on published dates is primarily dominated by analytical uncertainty associated with the measurement apparatus. The isotopic inventory of the rocks themselves can vary, however, and this is poorly constrained in general. The general messiness of rapid geological change during the Flood, coupled with AND, would cause additional natural variability. Studies to examine this could help determine how much inheritance and relaxation impact a particular magmatic system, and provide minimum and maximum bounds for a fully defined decay history function at various points in time.

When dealing with a radioisotope system which has multiple decays between the parent isotope and the final daughter isotope, such as the U/Pb system, dating is performed under the assumption that the sample has reached secular equilibrium. When this condition is reached,

then the amount of intermediate daughter isotopes remaining in the sample is directly controlled by parent decays since the longer half-life parent is the rate-limiting factor in growth of the intermediates. If secular equilibrium has been established by the time of measurement, then the ratios of the isotopes in the chain reach a steady-state, and dating can be done under the assumption that parent decays directly to the ultimate daughter isotope at the decay rate of the parent. Secular equilibrium is established after several half-lives of the intermediate daughter products have passed, sufficient for any initial excess to have decayed away. Secular equilibrium is an observable condition, but in most cases, it is assumed to be true rather than measured. Prior studies have shown that secular equilibrium is established in at least some cases (Deschamps et al., 2004). One caveat to consider is that the half-lives of long-lived intermediate daughter products are typically measured by first assuming that secular equilibrium has been reached, though it is possible to measure them directly without that assumption and achieve a generally similar value (Varga et al., 2016).

The vast majority of radioisotopes in the U/Pb system have sufficiently short half-lives to have established secular equilibrium in the time since the Flood, with four notable exceptions. In the radium series, ^{234}U has a half-life of 245,500 years, ^{230}Th has a half-life of 75,400 years, and ^{226}Ra has a half-life of 1,600 years. In the actinium series, ^{231}Pa has a half-life of 32,760 years (National Nuclear Data Center, 2008). It is possible that following the AND epoch, that samples would have an excess of these daughter products, causing the radiometric system to tick at an anomalously high rate until these isotopes were depleted. Several studies have documented significant excesses of ^{231}Pa in a wide variety of geodynamic settings (Asmerom et al., 2000, p. 293). Rioux et al. (2015, p. 144) acknowledge that their observed excess ^{231}Pa is likely the cause of the discordance in high precision U-Pb dates of mid ocean ridge zircons. They proposed preferential incorporation of Pa into zircon crystals during formation. The expected departure from secular equilibrium following AND depends on the chemical affinities of each of the elements (Kelemen et al., 2004, p. 629), as well as the relative change in the decay constants of parent and intermediate daughter during the epoch. This provides a unique window into how AND affected different isotopes. Standard radiometric analyses do not include measurements of these intermediate isotopes, and so the measurements are not common. These additional measurements should be prioritized to better constrain the nature of the underlying mechanism for AND and the amount of decay acceleration experienced.

Similarly, discordance between different radioisotopes systems provide constraints on the relative decay acceleration between the two isotopes. This information may also elucidate geophysical conditions that effect reservoir relaxation, establishing a basis to consider dates to be relatively comparable. Other geochronometers such as fission track dating and He diffusion provide evidence on *in situ* nuclear decay, so can constrain the impact of secondary processes.

With variable decay acceleration, symmetric analytical uncertainties will generally be asymmetric when corrected to absolute times via the inverse decay history function.

B. Broad outline of potential models

There is a diversity of opinion on how to correlate the Global Uniformitarian Chronostratigraphic Time Scale with the Flood year. However, most agree that at least Cambrian (541Ma) thru Cretaceous (66Ma) are Flood equivalent, yielding a minimum Flood radiometric range of 475 million years. Assuming this minimal consensus Flood radiometric range for the Flood leaves 4026 million radiometric years for the Antediluvian period and 66 million years for the modern period. Dividing each of these accumulated radiometric ages by Ussher's durations for each respective period of history (Ussher, 2003) gives the following time averaged nuclear decay accelerations:

$$\bar{\Xi}_{\text{Antediluvian}} \leq 2.4 \quad \text{Ma/year}$$
$$\bar{\Xi}_{\text{Flood}} \geq 480 \quad \text{Ma/year}$$
$$\bar{\Xi}_{\text{Modern}} \leq 0.015 \quad \text{Ma/year}$$

Even though there is more than 8 times as much accumulated radiometric age before the consensus Flood range, there is a much larger time period that this acceleration is averaged over, so the average acceleration is smaller. A portion of this earlier apparent acceleration could be due to a primordial signature as well. This leads to the conclusion that to first order, decay acceleration during the Flood must be pulse-like. This pulse would be even more significant if additional accumulated radiometric age is attributable to the Flood above the consensus Flood range. Even though there may be differences between models during the Flood, they are only going to be interesting at second order or lower, so it is natural to differentiate models primarily by how the extra radiometric range is distributed both during Antediluvian time, and the termination behavior. A potential model could be Flood-only, accounting for all the Precambrian accumulated decay during the time of the Flood. Other models may be Flood anticipatory, where AND is proposed to occur before the Flood, but only in direct association (lead-up) with it. Other potential model categories propose a significant primordial signature, or two pulses of AND at different times in history e.g., Creation/Flood. Models can also be described by their termination behavior as mid-Flood, end-Flood, or post-Flood.

C. Possible case study for reservoir relaxation

If the reservoir relaxation mechanism following AND described in this report has occurred in earth history, then one of the most apparent unique features that could potentially be observed is the behavior of geographically proximal, but chemically distinct post-Flood volcanic centers which would undergo differing rates of decay product release. If the stratigraphy of numerous distinct flows could be determined without reference to radiometric dates, then the nonlinear behavior of the reservoir relaxation might be determined. This would be manifest as dates decreasing opposite to stratigraphic position, and perhaps a transition point where one system measures younger for later times, and then begins to measure older for equivalent earlier times. See figure 5 for a contrived example. The benefit of studying a heterogeneous system like this is that rocks from both magma sources have been subject to the same decay history, and the reservoir relaxation can be determined without having established the decay history beforehand to correct eruption timelines. It may be possible to jointly solve for the relaxation parameters of both reservoirs simultaneously.

One possible location with the right criteria is the San Francisco Volcanic Field in Northern Arizona. This volcanic field is one of the most diverse and complex eruptive centers in North America. Volcanic features in the field include maars and tuff rings, numerous monogenetic scoria cones and lava flows, and six major intermediate to silicic volcanic centers comprising domes and a stratovolcano. The scoria cones have erupted along two main fault-controlled alignments north-south and northeast-southwest. A few of these scoria cones produced a final dacite or rhyolite dome in the center of the cone. The silicic centers are concentrated on a different northeast-southwest line, thought to represent buried Paleozoic fault traces (Valentine et al., 2021).

Lava types erupted from over 600 vents range in composition from picro-basalt to trachyte, and rhyolite along a generally calc-alkalic trend. Some of the lavas have the distinctive elemental ratios that are generally considered indicative of subduction zone magma even though the volcanic field is far away from any recently active subduction zones. The magma sources are diverse, including mafic asthenospheric melts as well as lower crust derived melts. Magma diversity has been effected by variable crustal melting of garnet-bearing upper mantle, mixing between different mantle source domains, extreme crystal fractionation, mixing of rhyolite and mafic melts, crustal anatexis, and assimilation (Arculus and Gust, 1995).

San Francisco Mountain ("the Peaks", figure 9) is the most prominent volcano in northern Arizona, its summit being the highest point in the state. It is located at the junction of three of the major fault alignments that provide structural control for the volcanic field. The present mountain peaks are remnants of two original stratocones which underwent sector collapse towards the northwest, leaving behind a substantial debris fan and an interior valley known as the Inner Basin. Numerous intermediate to silicic flows, dikes, and domes comprise the structure of San Francisco Mountain, and many of these at different structural depths are exposed in the inner basin. This provides strong stratigraphic control for these flows. Several satellite volcanoes are near to San Francisco Mountain and have flows that overlap. Additionally, numerous radiometric dates have been obtained for many of these individual flows. Figure 10 shows dates referenced by Holm (2021) plotted against the stratigraphic position of the relevant flows. In general, the more recent Ar-Ar dates do not agree with the K-Ar ages, either up or down. Due to the large uncertainties, it is possible to select a consistent sequence of dates that would agree with the stratigraphic ordering. The most likely ages, however, have inconsistencies where a younger flow dates older. Additionally, dacite dates may be on the whole older than the other lithology types. The Ar-Ar results are also strikingly different, seeming to indicate much less time between eruptive phases than the equivalent K-Ar ages. The size of the measurement uncertainties prevents making conclusions at this time, but this locality should be investigated with more high-quality radiometric measurements using multiple methodologies. Samples should be taken from all volcanic rocks exposed on San Francisco Mountain, Mount Elden, and the Dry Lake Hills that are able to be fit into the regional stratigraphy. Additionally, samples of basalt and dacite should be taken from the monogenetic cones which erupted both types (Strawberry and O'Neill craters). High quality radiometric analyses should be done on all of these samples including Ar-Ar and U-Pb methods. These would be evaluated against the stratigraphy for out-of-order dating based on composition. Out-of-order dating has occasionally been observed in other settings and has been explained by various mechanisms including Ar loss through recoil effects (Baksi, 1994). Studies like these should also be evaluated in depth.

V. CONCLUSION

The 2005 RATE study fundamentally changed the way that radiometric dates should be interpreted by showing conclusive evidence for at

Figure 9. San Francisco Mountain ("The Peaks") in Northern Arizona is a complex stratovolcano with lava types ranging from basalt to trachyte, andesite, dacite, and rhyolite, many of which overlap in stratigraphically discernible relationships. H - Humphreys Peak, A - Agassiz Peak, F - Fremont Peak, D - Doyle Peak, S - Schultz Peak. The lake bed and hills in the foreground are a tuff ring known as Dry Lake.

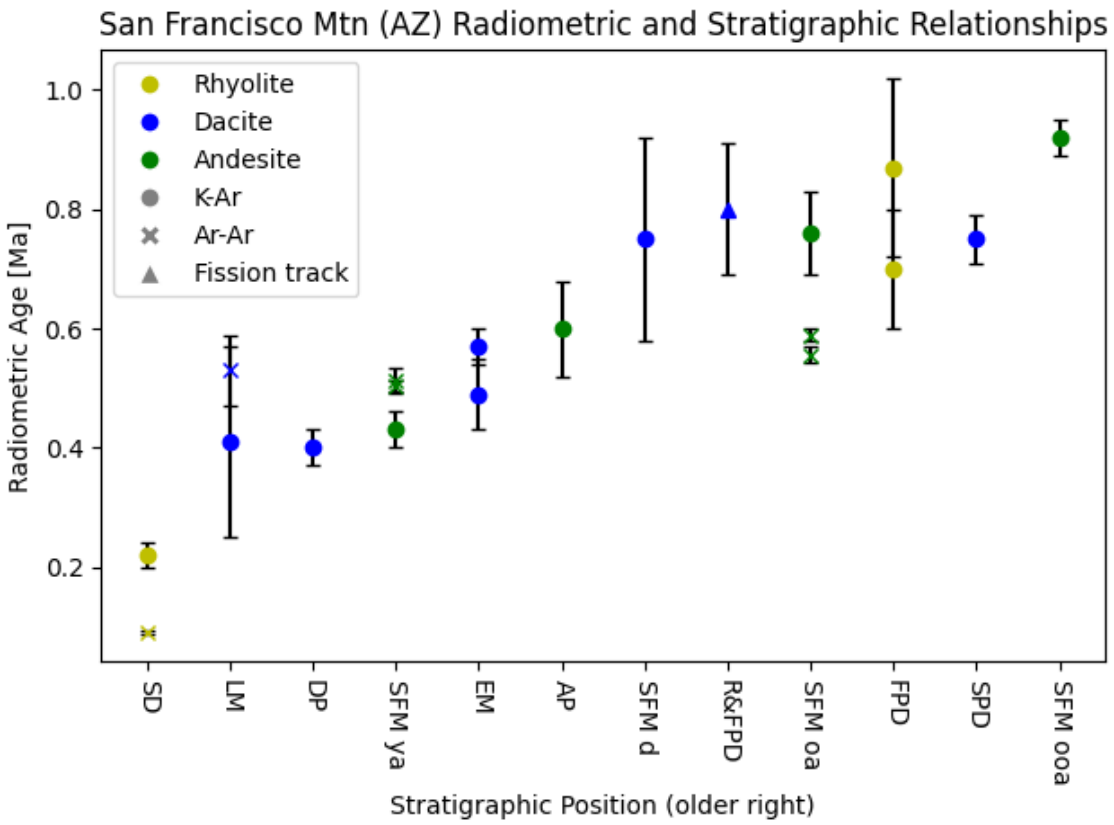

Figure 10. Radiometric dates from sources in the San Francisco Volcanic field plotted in stratigraphic order. Although the uncertainties are high, there is a possibility of different rock types exhibiting differing radiometric behavior. Rocks sampled in order form left to right are: SD-Sugarloaf dome, LM-Lockett Meadow dacite, DP-Doyle Peak dacite, SFM ya-younger andesite of San Francisco Mountain, EM-Elden Mountain domes, AP-Agassiz Peak andesite, SFM d-dacite of San Francisco Mountain, R&FP-domes and flows of Reese and Fremont Peaks, SFM oa-older andesite of San Francisco Mountain, FPD-Fremont Peak dome, SPD-Schultz Peak domes, SFM ooa-(older) older andesite of San Francisco Mountain. Circles are K-Ar dates from Wolfe et al., 1987, diamonds are Ar-Ar dates from Karátson et al., 2010 and Morgan et al., 2010, triangles are fission-track ages from Ulrich and Bailey, 1987.

least one episode of AND in the past. While providing the answers to some longstanding questions about the place of radiometric dating in Biblical history, it raised new questions regarding the follow-on implications that have hitherto been unexplored. Relatively accurate radiometric dates have been in use in the published record since that time, and it has been recognized that if relative ordering of dates is valid, then there should theoretically be a valid method of converting these ages into historical dates. I have proven this to be the case in theorem 1. Furthermore, I have established the relations necessary to construct an absolute dating framework within Biblical history, identified the conditions under which it can be used, and described conditions needed for relative dating. From these relations, I have also shown that magma reservoir relaxation — the reduction in apparent radiometric age of successive radiometrically datable rocks sourced from the reservoir over time — is a natural and unavoidable consequence of an episode of AND. Due to the extreme excess of radiogenic daughter products, AND causes anomalous inheritance despite small partition ratios between crystal and melt in a magma. This direct consequence of AND is a challenge to characterize which is likely the reason that a general radiometric history model able to accurately convert between radiometric ages and historical dates has for so long not been formulated. Relative radiometric dating is also affected except in restricted circumstances where the effects of reservoir relaxation cancel out. Constructing and constraining a model will take multiple studies and require observations that are not often undertaken in conventional studies. The reservoir relaxation mechanism easily explains the measured secular change of radiometric dates of post-Flood volcanic features without needing an extended AND ramp down. It also explains why most modern volcanoes measure properly at zero age but why some volcanoes repeatably do not. I make a prediction based upon the action of the reservoir relaxation mechanism and propose a fertile location to test the prediction. Finally, I provide a pathway for future research defining models of decay histories and understanding further implications of the AND epoch. The realities of AND make absolute radiometric dating difficult, but the effort required is well worth the reward of having such a powerful tool available to study the earth and solar system within a Biblical framework.

NOMENCLATURE

AND	Accelerated Nuclear Decay
RATE	Radioisotopes and the Age of The Earth
He	Helium
K	Potassium
Ar	Argon
Pb	Lead
Ra	Radium

Pa	Protactinium
Th	Thorium
U	Uranium
ka	kilo-annum (thousands of years before epoch)
Ma	Mega-annum (millions of years before epoch)
Ga	Giga-annum (billions of years before epoch)
YBP	Years before present

REFERENCES

Arculus, R.J. and D.A. Gust. 1995. Regional petrology of the San Francisco Volcanic Field, Arizona, USA. *Journal of Petrology* 36, no. 3:827–861. DOI:10.1093/petrology/36.3.827.

Asmerom, Y., H. Cheng, R. Thomas, M. Hirschmann, and R.L. Edwards. 2000. Melting of the earth's lithospheric mantle inferred from protactinium– thorium–uranium isotopic data. *Nature* 406, no. 6793:293–296. DOI:10.1038/35018550.

Austin, S.A. 1996. Excess argon within mineral concentrates from the new dacite lava dome at Mount St Helens volcano. *TJ* 10, no. 3:335–343.

Austin, S.A. and A.A. Snelling. 1998. Discordant potassium-argon model and isochron "ages" for Cardenas Basalt (middle Proterozoic) and associated diabase of eastern Grand Canyon, Arizona. In Walsh (1998), pp. 35–51.

Baksi, A.K. 1994. Geochronological studies on whole-rock basalts, Deccan Traps, India: evaluation of the timing of volcanism relative to the K-T boundary. *Earth and Planetary Science Letters* 121, no. 1:43–56. DOI:10.1016/0012-821X(94)90030-2.

Ballentine, C.J., R. Burgess, and B. Marty. 2002. Tracing Fluid Origin, Transport and Interaction in the Crust. *Reviews in Mineralogy and Geochemistry* 47, no. 1:539–614. DOI:10.2138/rmg.2002.47.13.

Ballentine, C.J. and P.G. Burnard. 2002. Production, Release and Transport of Noble Gases in the Continental Crust. *Reviews in Mineralogy and Geochemistry* 47, no. 1:481–538. DOI:10.2138/rmg.2002.47.12.

Baumgardner, J. 2005. 14C evidence for a recent global flood and a young earth. In Vardiman et al. (2005), pp. 587–630.

Baumgardner, J. 2012. Do radioisotope methods yield trustworthy relative ages for the earth's rocks? *Journal of Creation* 26, no. 3:68–75.

Bea, F., I. Morales, J.F. Molina, P. Montero, and A. Cambeses. 2021. Zircon stability grids in crustal partial melts: implications for zircon inheritance. *Contributions to Mineralogy and Petrology* 176, no. 3:18. DOI:10.1007/s00410-021-01772-x.

Bini, G., G. Chiodini, S. Caliro, F. Tassi, O. Vaselli, A.L. Rizzo, S. Mollo, G.E. Vougioukalakis, and O. Bachmann. 2022. Nitrogen, helium, and argon reveal the magmatic signature of fumarole gases and episodes of outgassing from upper-crustal magma reservoirs: The case of the Nisyros caldera (Aegean Arc, Greece). *Geochimica et Cosmochimica Acta* 335:68–84. DOI:10.1016/j.gca.2022.08.028.

Byrne, D., M. Broadley, S. Halldórsson, E. Ranta, A. Ricci, R. Tyne, A. Stefánsson, C. Ballentine, and P. Barry. 2021. The use of noble gas isotopes to trace subsurface boiling temperatures in Icelandic geothermal systems. *Earth and Planetary Science Letters* 560:116805. DOI:10.1016/j.epsl.2021.116805.

Chaffin, E.F. 2005. Accelerated decay: Theoretical considerations. In Vardiman et al. (2005), pp. 525–586.

Cheng, A., B. Sherwood Lollar, O. Warr, G. Ferguson, E. Idiz, S.O. Mundle, P.H. Barry, D.J. Byrne, J.C. Mabry, and C.J. Ballentine. 2021. Determining the role of diffusion and basement flux in controlling 4He distribution in sedimentary basin fluids. *Earth and Planetary Science Letters* 574:117175. DOI:10.1016/j.epsl.2021.117175.

Dalrymple, G. 1969. 40Ar/36Ar analyses of historic lava flows. *Earth and Planetary Science Letters* 6, no. 1:47–55. DOI:10.1016/0012-821X(69)90160-5.

Dalrymple, G.B. and J.G. Moore. 1968. Argon-40: Excess in submarine pillow basalts from Kilauea volcano, Hawaii. *Science* 161, no. 3846:1132–1135. DOI:10.1126/science.161.3846.1132.

Damon, P., A. Laughlin, and J. Percious. 1967. Problem of excess argon-40 in volcanic rocks. In *Radioactive dating and methods of low-level counting. Proceedings of a symposium*.

Day, J.M. and D.R. Hilton. 2020. Heterogeneous mantle-derived helium isotopes in the Canary Islands and other ocean islands. *Geology* 49, no. 2:120–124. DOI:10.1130/G47676.1.

Deschamps, P., C. Hillaire-Marcel, J.L. Michelot, R. Doucelance, B. Ghaleb, and S. Buschaert. 2004. $^{234}U/^{238}U$ disequilibrium along stylolitic discontinuities in deep Mesozoic limestone formations of the eastern Paris basin: evidence for discrete uranium mobility over the last 1–2 million years. *Hydrology and Earth System Sciences* 8, no. 1:35–46. DOI:10.5194/hess-8-35-2004.

Esser, R., W. McIntosh, M. Heizler, and P. Kyle. 1997. Excess argon in melt inclusions in zero-age anorthoclase feldspar from Mt. Erebus, Antarctica, as revealed by the 40Ar/39Ar method. *Geochimica et Cosmochimica Acta* 61, no. 18:3789–3801. DOI:10.1016/S0016-7037(97)00287-1.

Fisher, D.E. 1972. U/He ages as indicators of excess argon in deep sea basalts. *Earth and Planetary Science Letters* 14, no. 2:255–258. DOI:10.1016/0012-821X(72)90016-7.

Froede, C.R., Jr and A.J. Akridge. 2012. RATE Study: Questions regarding accelerated nuclear decay and radiometric dating. *Creation Research Society Quarterly* 49, no. 1:68–75.

Geist, D., K. Harpp, P. Oswald, P. Wallace, I. Bindeman, and B. Christensen. 2021. Hekla revisited: fractionation of a magma body at historical timescales. *Journal of Petrology* 62, no. 8. DOI:10.1093/petrology/egab001.

Giorgis, D., M. Cosca, and S. Li. 2000. Distribution and significance of extraneous argon in UHP eclogite (Sulu terrain, China): insight from in situ 40Ar/39Ar UV-laser ablation analysis. *Earth and Planetary Science Letters* 181, no. 4:605–615. DOI:10.1016/S0012-821X(00)00221-1.

Graham, D.W. 2002. Noble gas isotope geochemistry of mid-ocean ridge and ocean island basalts: Characterization of mantle source reservoirs. *Reviews in Mineralogy and Geochemistry* 47, no. 1:247–317. DOI:10.2138/rmg.2002.47.8.

Harrison, T.M., M.T. Heizler, O.M. Lovera, Chen Wenji, and M. Grove. 1994. A chlorine disinfectant for excess argon released from K-feldspar during step heating. *Earth and Planetary Science Letters* 123, no. 1:95–104. DOI:10.1016/0012-821X(94)90260-7.

Heber, V.S., R.A. Brooker, S.P. Kelley, and B.J. Wood. 2007. Crystal–melt partitioning of noble gases (helium, neon, argon, krypton, and xenon) for olivine and clinopyroxene. *Geochimica et Cosmochimica Acta* 71, no. 4:1041–1061. DOI:10.1016/j.gca.2006.11.010.

Hoang, H., K.H. Ho, A. Battani, M. Pujol, and G. Galliero. 2021. On elemental and isotopic fractionation of noble gases in geological fluids by molecular diffusion. *Geochimica et Cosmochimica Acta* 315:172–184. DOI:10.1016/j.gca.2021.09.002.

Holm, R.F. 2021. Petrography, geochemistry, and volcanogenic development

of the San Francisco Mountain volcanic system, northern Arizona. Arizona Geological Survey, Contributed Report CR-21-C.

Holm-Alwmark, S., F. Jourdan, L. Ferrière, C. Alwmark, and C. Koeberl. 2021. Resolving the age of the Puchezh-Katunki impact structure (Russia) against alteration and inherited 40Ar* – No link with extinctions. *Geochimica et Cosmochimica Acta* 301:116–140. DOI:10.1016/j.gca.2021.03.001.

Hu, R.G., X.J. Bai, J. Wijbrans, F. Brouwer, Y.L. Zhao, and H.N. Qiu. 2018. Occurrence of excess 40Ar in amphibole: Implications of 40Ar/39Ar dating by laser stepwise heating and in vacuo crushing. *Journal of Earth Science* 29, no. 2:416–426. DOI:10.1007/s12583-017-0947-x.

Humphreys, D.R. 2014. Magnetized moon rocks shed light on Precambrian mystery. *Journal of Creation* 28, no. 3:51–60.

Hung, C.Y. 2008. A realistic simulation model for uranium series geochronological dating. *Creation Research Society Quarterly* 45, no. 1:40–52.

Jackson, C.R., C.D. Williams, Z. Du, N.R. Bennett, S. Mukhopadhyay, and Y. Fei. 2021. Incompatibility of argon during magma ocean crystallization. *Earth and Planetary Science Letters* 553:116598. DOI:10.1016/j.epsl.2020.116598.

Karátson, D., T. Telbisz, and B.S. Singer. 2010. Late-stage volcano geomorphic evolution of the Pleistocene San Francisco mountain, Arizona (USA), based on high-resolution DEM analysis and 40Ar/39Ar chronology. *Bulletin of Volcanology* 72, no. 7:833–846.

Karpinskiy, T., L. Shanin, and I. Borisevich. 1966. Artificial injection of argon in mica, olivine and pyroxene. *International Geology Review* 8, no. 7:768–769. DOI:10.1080/00206816609474336.

Kawaguchi, M., T. Hasenaka, K.T. Koga, E.F. Rose-Koga, A. Yasuda, N. Hokanishi, Y. Mori, K. Shimizu, and T. Ushikubo. 2021. Persistent gas emission originating from a deep basaltic magma reservoir of an active volcano: the case of Aso volcano, Japan. *Contributions to Mineralogy and Petrology* 176, no. 1:6. DOI:10.1007/s00410-020-01761-6.

Kelemen, P.B., K. Hanghøj, and A.R. Greene. 2004. One view of the geochemistry of subduction-related magmatic arcs, with an emphasis on primitive andesite and lower crust. In R.L. Rudnick, H.D. Holland, and K.K. Turekian (editors) *Treatise on geochemistry*, volume 3, p. 593–660. Kidlington, Oxford: Elsevier/Pergamon.

Kelley, S. 2002a. Excess argon in K–Ar and Ar–Ar geochronology. *Chemical Geology* 188, no. 1:1–22. DOI:10.1016/S0009-2541(02)00064-5.

Kelley, S. 2002b. K-Ar and Ar-Ar Dating. *Reviews in Mineralogy and Geochemistry* 47, no. 1:785–818. DOI:10.2138/rmg.2002.47.17.

Krummenacher, D. 1970. Isotopic composition of argon in modern surface volcanic rocks. *Earth and Planetary Science Letters* 8, no. 2:109–117. DOI:10.1016/0012-821X(70)90159-7.

Lamy-Chappuis, B., C.A. Heinrich, T. Driesner, and P. Weis. 2020. Mechanisms and patterns of magmatic fluid transport in cooling hydrous intrusions. *Earth and Planetary Science Letters* 535:116111. DOI:10.1016/j.epsl.2020.116111.

Lee, J.K.W., T.C. Onstott, and J.A. Hanes. 1990. An 40Ar/39Ar investigation of the contact effects of a dyke intrusion, Kapuskasing structural zone, Ontario. *Contributions to Mineralogy and Petrology* 105, no. 1:87–105. DOI:10.1007/BF00320969.

McDougall, I. and T.M. Harrison. 1999. *Geochronology and Thermochronology by the 40Ar/39Ar Method*. Oxford University Press, 2nd edition.

McDougall, I., H. Polach, and J. Stipp. 1969. Excess radiogenic argon in young subaerial basalts from the Auckland volcanic field, New Zealand. *Geochimica et Cosmochimica Acta* 33, no. 12:1485–1520. DOI:10.1016/0016-7037(69)90152-5.

Merrihue, C. and G. Turner. 1966. Potassium-argon dating by activation with fast neutrons. *Journal of Geophysical Research (1896-1977)* 71, no. 11:2852–2857. DOI:10.1029/JZ071i011p02852.

Morgan, P., J.H. Sass, and W. Duffield. 2010. Geothermal resources evaluation program of the eastern San Francisco volcanic field, Arizona. Arizona Geological Survey, Contributed Report CR-10-D.

National Nuclear Data Center, B.N.L. 2008. Nudat (nuclear structure and decay data).

https://www.nndc.bnl.gov/nudat3/.

Noble, C.S. and J.J. Naughton. 1968. Deep-ocean basalts: Inert gas content and uncertainties in age dating. *Science* 162, no. 3850:265–267. DOI:10.1126/science.162.3850.265.

Nteme, J., S. Scaillet, P. Brault, and L. Tassan-Got. 2022. Atomistic simulations of 40Ar diffusion in muscovite. *Geochimica et Cosmochimica Acta* 331:123–142. DOI:10.1016/j.gca.2022.05.004.

Oard, M.J. 2013. Can the relative timing of radioisotope dates be applied to biblical geology? *Journal of Creation* 27, no. 2:112–119.

Oard, M.J. 2021. Much greater cosmic rays during the Ice Age and before. *Creation Research Society Quarterly* 58, no. 1:30–48.

Overman, R.L. 2013. The temporal, geographical, and geological ubiquity of excess argon with a young-earth analysis. In M. Horstemeyer (editor) *Proceedings of the 7th International Conference on Creationism*. Pittsburgh, Pennsylvania: Creation Science Fellowship.

Ozawa, A., T. Tagami, and H. Kamata. 2006. Argon isotopic composition of some Hawaiian historical lavas. *Chemical Geology* 226, no. 1:66–72. DOI:10.1016/j.chemgeo.2005.10.001.

Pickles, C., S. Kelley, S. Reddy, and J. Wheeler. 1997. Determination of high spatial resolution argon isotope variations in metamorphic biotites. *Geochimica et Cosmochimica Acta* 61, no. 18:3809–3833. DOI:10.1016/S0016-7037(97)00289-5.

Rama, S.N.I., S.R. Hart, and E. Roedder. 1965. Excess radiogenic argon in fluid inclusions. *Journal of Geophysical Research (1896-1977)* 70, no. 2:509–511. DOI:10.1029/JZ070i002p00509.

Reddy, S.M., S.P. Kelley, and J. Wheeler. 1996. A 40Ar/39Ar laser probe study of micas from the Sesia zone, Italian Alps: implications for metamorphic and deformation histories. *Journal of Metamorphic Geology* 14, no. 4:493–508. DOI:10.1046/j.1525-1314.1996.00338.x.

Reed, J.K. and C. Froede. 2010. Can "relative" radiometric dating help refine biblical chronology? *Creation Research Society Quarterly* 47, no. 1:71–73.

Renne, P.R., W.S. Cassata, and L.E. Morgan. 2009. The isotopic composition of atmospheric argon and 40Ar/39Ar geochronology: Time for a change? *Quaternary Geochronology* 4, no. 4:288–298. DOI:10.1016/j.quageo.2009.02.015.

Renne, P.R., W.D. Sharp, A.L. Deino, G. Orsi, and L. Civetta. 1997. $^{40}Ar/^{39}Ar$ dating into the historical realm: Calibration against Pliny the Younger. *Science* 277, no. 5330:1279–1280. DOI:10.1126/science.277.5330.1279.

Rioux, M., S. Bowring, M. Cheadle, and B. John. 2015. Evidence for initial excess 231Pa in mid-ocean ridge zircons. *Chemical Geology* 397:143–156. DOI:10.1016/j.chemgeo.2015.01.011.

Rust, A., K. Cashman, and P. Wallace. 2004. Magma degassing buffered by vapor flow through brecciated conduit margins. *Geology* 32, no. 4:349–352. DOI:10.1130/G20388.2.

Scibiorski, E., F. Jourdan, K. Mezger, E. Tohver, and H. Vollstaedt. 2021. Cryptic excess argon in metamorphic biotite: Anomalously old 40Ar/39Ar plateau dates tested with Rb/Sr thermochronology and Ar diffusion modelling. *Geochimica et Cosmochimica Acta* 315:1–23. DOI:10.1016/j.gca.2021.09.017.

Sherlock, S. and S. Kelley. 2002. Excess argon evolution in HP–LT rocks: a UVLAMP study of phengite and K-free minerals, NW Turkey. *Chemical Geology* 182, no. 2:619–636. DOI:10.1016/S0009-2541(01)00345-X.

Shormann, D.E. 2013. 40Ar/39Ar calibration against Novarupta: no good reason to believe in millions of years. *Creation Research Society Quarterly* 50, no. 1:13–24.

Snelling, A.A. 1998. The cause of anomalous potassium-argon "ages" for recent andesite flows at Mt Ngauruhoe, New Zealand, and the implications for potassium-argon "dating". In Walsh (1998), pp. 503–525.

Snelling, A.A. 2005. Radiohalos in granites: Evidence for accelerated nuclear decay. In Vardiman et al. (2005), pp. 101–208.

Snelling, A.A. 2008. Testing the hydrothermal fluid transport model for polonium radiohalo formation: The Thunderhead Sandstone, Great Smoky Mountains, Tennessee- North Carolina. *Answers Research Journal* 1:53–64.

Snelling, A.A. 2014. Radioisotope dating of meteorites: I. The Allende CV3 carbonaceous chondrite. *Answers Research Journal* 7:103–145.

Torgersen, T., B. Kennedy, H. Hiyagon, K. Chiou, J. Reynolds, and W. Clarke. 1989. Argon accumulation and the crustal degassing flux of 40Ar in the Great Artesian Basin, Australia. *Earth and Planetary Science Letters* 92, no. 1:43–56. DOI:10.1016/0012-821X(89)90019-8.

Ubide, T., P. Larrea, L. Becerril, and C. Galé. 2021. Volcanic plumbing filters on ocean-island basalt geochemistry. *Geology* 50, no. 1:26–31. DOI:10.1130/G49224.1.

Ulrich, G. and N. Bailey. 1987. Geologic map of the SP Mountain part of the San Francisco volcanic field, north-central Arizona. U. S. Geological Survey, miscellaneous field studies map MF-1956. 1:50,000.

Ussher, J. 2003. *The Annals of the World*. EBL-Schweitzer. New Leaf Publishing Group, Incorporated.

Valentine, G.A., M.H. Ort, and J.A. Cortés. 2021. Quaternary basaltic volcanic fields of the American Southwest. *Geosphere* 17, no. 6:2144–2171. DOI:10.1130/GES02405.1.

Vardiman, L., A.A. Snelling, and E.F. Chaffin (editors). 2005. *Radioisotopes and the Age of the Earth: Results of a Young-Earth Creationist Research Initiative*. El Cajon, California: Institute for Creation Research and Chino Valley, Arizona: Creation Research Society.

Varga, Z., A. Nicholl, M. Wallenius, and K. Mayer. 2016. Remeasurement of 234U half-life. *Analytical Chemistry* 88, no. 5:2763–2769. DOI:10.1021/acs.analchem.5b04370.

Walsh, R.E. (editor). 1998. *Proceedings of the 4th International Conference on Creationism*. Pittsburgh, Pennsylvania: Creation Science Fellowship.

Watkins, J., J. Gardner, and K. Befus. 2017. Nonequilibrium degassing, regassing, and vapor fluxing in magmatic feeder systems. *Geology* 45, no. 2:183–186. DOI:10.1130/G38501.1.

Watson, E., D. Chemiak, J. Hanchar, T. Harrison, and D. Wark. 1997. The incorporation of Pb into zircon. *Chemical Geology* 141, no. 1:19–31. DOI:10.1016/S0009-2541(97)00054-5.

Wolfe, E., G. Ulrich, R. Holm, R. Moore, and C. Newhall. 1987. Geologic map of the central part of the San Francisco volcanic field, north-central Arizona. U. S. Geological Survey, miscellaneous field studies map MF-1959. 1:50,000.

Zelenski, M., A. Simakin, Y. Taran, V. Kamenetsky, and N. Malik. 2021. Partitioning of elements between high-temperature, low-density aqueous fluid and silicate melt as derived from volcanic gas geochemistry. *Geochimica et Cosmochimica Acta* 295:112–134. DOI:10.1016/j.gca.2020.12.011.

APPENDIX: SUPPLEMENTAL DERIVATIONS

A. Acceleration factor and decay history function

Given the differential relation in equation 1:

$$\frac{\mathrm{d}P}{\mathrm{d}t} = -\lambda(t)P$$

This is a first-order linear ordinary differential equation that is separable, so the solution is easily found by separating the variables and integrating. We will integrate the right-hand side from time 0 to t and the left-hand side from the initial number of parent atoms, P_0, to the present number.

$$\begin{aligned}\int_{P_0}^{P}\frac{1}{P}\mathrm{d}P &= \int_0^t -\lambda(\tau)\mathrm{d}\tau \\ \ln\left|\frac{P}{P_0}\right| &= \int_0^t -\lambda(\tau)\mathrm{d}\tau \\ P &= P_0\exp\left(\int_0^t -\lambda(\tau)\mathrm{d}\tau\right)\end{aligned}$$

Bearing in mind that $P + D = P_0$,

$$\int_0^t \lambda(\tau)\mathrm{d}\tau = \ln\left(1+\frac{D}{P}\right). \quad (22)$$

The observables in equation 2 can be equated with equation 22 to obtain

$$t_m = H(t) = \int_0^t \frac{\lambda(\tau)}{\lambda_0}\mathrm{d}\tau. \quad (23)$$

B. Reservoir relaxation

Given the differential relation in equation 11:

$$\frac{\mathrm{d}p_r}{\mathrm{d}t} = -\beta\left(H\left(t_R^*|_{t_s}\right) - H(t) - p_r(t)\right)$$

The solution of this separable, first-order linear ordinary differential

equation is as follows:

$$\begin{aligned}
\dot{p_r} - \beta p_r &= -\beta\left(H\left(t_R^*|_{t_s}\right) - H(t)\right) \\
e^{-\beta t}\dot{p_r} + \frac{\mathrm{d}e^{-\beta t}}{\mathrm{d}t} p_r &= -\beta e^{-\beta t}\left(H\left(t_R^*|_{t_s}\right) - H(t)\right) \\
\frac{\mathrm{d}e^{-\beta t} p_r}{\mathrm{d}t} &= -\beta e^{-\beta t} H\left(t_R^*|_{t_s}\right) + \beta e^{-\beta t} H(t) \\
e^{-\beta t} p_r &= e^{-\beta t} H\left(t_R^*|_{t_s}\right) + \beta \int_{t_s}^{t} e^{-\beta\tau} H(\tau)\mathrm{d}\tau - C \\
p_r &= H\left(t_R^*|_{t_s}\right) - \beta e^{\beta t} \int_{t}^{t_s} e^{-\beta\tau} H(\tau)\mathrm{d}\tau - C e^{\beta t}
\end{aligned}$$

To solve for the constant of integration, it is recognized that the size of the perturbation at the time of reservoir formation $p(t_s) = 0$. Conveniently, the integral term is also 0.

$$\begin{aligned}
p_r(t) &= H\left(t_R^*|_{t_s}\right) - \beta e^{\beta t} \int_{t}^{t_s} e^{-\beta\tau} H(\tau)\mathrm{d}\tau - C e^{\beta t} \\
&= 0 \\
C &= H\left(t_R^*|_{t_s}\right) e^{-\beta t_s} \\
p_r(t) &= H\left(t_R^*|_{t_s}\right)\left(1 - e^{-\beta(t_s - t)}\right) \\
&\quad -\beta e^{\beta t} \int_{t}^{t_s} e^{-\beta\tau} H(\tau)\mathrm{d}\tau
\end{aligned}$$

THE AUTHOR

Nathan Mogk has been researching young-earth geology and related topics since 2013. He has a Master's degree in systems engineering, and undergraduate degrees in materials science and mathematics from an Arizona state university. He currently lives in Arizona, and has been working on field observations to fill in the gaps of knowledge that exist about how the Genesis Flood has affected the rocks in this iconic region. He also pursues matters of systematics and models that have broad application to young-earth geology.